Journal of Controlled Release 389 (2026) 114414

Contents lists available at ScienceDirect

Journal of Controlled Release

journal homepage: www.elsevier.com/locate/jconrel

Combination of ionizable lipids with oleic acid and vitamin E scaffolds for RNA cancer vaccine delivery

Jessica Anindita [a,b,1], Hiroki Tanaka [a,*,1], Ryotaro Oyama [a,b], Atsuya Matsumaru [a], Yuta Nakai [c], Kota Tange [c], Koji Nagaoka [d], Hideyuki Nakanishi [e,f], Takeshi Kawamura [g,h], Toshiya Tanaka [h], Takefumi Yamashita [h,i], Akihiro Kuroda [j], Sachiyo Nomura [g,j,k], Hiroto Hatakeyama [b], Keiji Itaka [e,f], Tatsuhiko Kodama [h], Kazuhiro Kakimi [d], Hidetaka Akita [a,*]

[a] Laboratory of DDS Design and Drug Disposition, Graduate School of Pharmaceutical Sciences, Tohoku University, 6-3, Aoba, Aramaki, Aoba-ku, Sendai City, Miyagi 980-8578, Japan
[b] Laboratory of DDS Design and Drug Disposition, Graduate School of Pharmaceutical Sciences, Chiba University, 1-8-1, Inohana, Chuo-ku, Chiba 260-0856, Japan
[c] Life Science Research Laboratory, NOF CORPORATION, 3-3 Chidori-cho, Kawasaki-ku, Kawasaki City, Kanagawa 210-0865, Japan
[d] Department of Immunology, Kindai University, Faculty of Medicine, 377-2 Ohnohigashi, Osakasayama, Osaka 589-0014, Japan
[e] Department of Biofunction Research, Laboratory for Biomaterials and Bioengineering, Institute of Integrated Research, Institute of Science Tokyo, 2-3-10 Kanda-Surugadai, Chiyoda-ku, Tokyo 101-0062, Japan
[f] Clinical Biotechnology Team, Center for Infectious Disease Education and Research (CiDER), Osaka University, 1-10 Yamadaoka, Suita City, Osaka 565-0871, Japan
[g] Isotope Science Center, The University of Tokyo, 2-11-16 Yayoi, Bunkyo-Ku, Tokyo 113-0032, Japan
[h] Department of Physical Chemistry, School of Pharmacy and Pharmaceutical Sciences, Hoshi University, 2-4-41 Ebara, Shinagawa-ku, Tokyo 142-8501, Japan
[i] Laboratories for Systems Biology and Medicine, Research Center for Advanced Science and Technology, The University of Tokyo, 4-6-1 Komaba, Meguro-ku, Tokyo 153-8904, Japan
[j] Department of Gastrointestinal Surgery, Graduate School of Medicine, The University of Tokyo, 7-3-1 Hongo, Bunkyo-Ku, Tokyo 113-8655, Japan
[k] Department of Clinical Pharmaceutical Sciences, School of Pharmacy and Pharmaceutical Sciences, Hoshi University, 2-4-41 Ebara, Shinagawa-Ku, Tokyo 142-8501, Japan

ARTICLE INFO

Keywords:
Lipid nanoparticle
Vitamin E
mRNA vaccine
Neoantigen cancer vaccine

ABSTRACT

RNA vaccines based on lipid nanoparticles (LNPs) encapsulating in vitro transcribed mRNA (IVT-mRNA) are a successful but evolving vaccine modality. It has been increasingly recognized that LNPs, which are mainly composed of ionizable lipids, have two roles in the action of RNA vaccines: delivering mRNA into the cytoplasm by overcoming the endosomal membrane and stimulating the innate immune system as an adjuvant. In this study, we report the development of LNPs with enhanced capability to induce cellular immunity by using a combination of ionizable lipids: one containing an oleic scaffold with high transfection activity (ssPalmO-Phe; SS-OP) and the other containing a vitamin E scaffold with high adjuvant activity (ssPalmE; SS-EC), referred to as $LNP_{OP/EC}$. The formulation's efficacy was evaluated in tumor-bearing mice, focusing on immune responses and tumor suppression. The results showed that the inclusion of vitamin E moieties in $LNP_{OP/EC}$ significantly enhanced cellular immune responses and suppressed tumor growth in an E.G7-OVA tumor-bearing mouse model. Additionally, it demonstrated robust activation of reactive $CD8^+$ T cells specifically recognizing the neoantigens mCdt1, mScarb2, and mZfp106, which are expressed in YTN16 murine gastric cells. Suppression of YTN16 tumors was also observed using $LNP_{OP/EC}$. The study suggests that $LNP_{OP/EC}$ is a viable platform for RNA-based cancer vaccines, offering a potent combination of gene expression and immune stimulation.

1. Introduction

Messenger RNA (mRNA) vaccines utilize the body's cellular machinery to produce target antigen proteins, thereby activating antigen-specific immune responses [1,2]. The encoded antigen can be readily selected by designing the sequence of the in vitro-transcribed

* Corresponding authors.
E-mail addresses: hiroki.tanaka.e1@tohoku.ac.jp (H. Tanaka), hidetaka.akita.a4@tohoku.ac.jp (H. Akita).
[1] These authors contributed equally to this study.

https://doi.org/10.1016/j.jconrel.2025.114414
Received 17 October 2025; Received in revised form 13 November 2025; Accepted 15 November 2025
Available online 17 November 2025

messenger RNA (IVT-mRNA), offering flexibility for both prophylactic and therapeutic vaccine applications in clinical practice. mRNA vaccines employing lipid nanoparticles (LNPs) have been widely applied in cancer vaccine development, representing an innovative immunotherapy approach that stimulates the immune system to specifically recognize and eliminate tumor cells. The antigens of cancer cells are broadly categorized into tumor-associated antigens (TAAs) and neoantigens. TAAs are overexpressed or aberrantly expressed in cancer tissues compared with normal tissues. Therefore, they can be used as selective markers/targets for cancer therapy. However, their presence in normal tissues can lead to immune tolerance, reducing the effectiveness of the immune response. On the other hand, neoantigens are foreign proteins absent in normal tissue, thus representing ideal targets for the development of personalized cancer vaccines (PCVs) [3–5]. Personalized mRNA neoantigen vaccines have been extensively studied, and several are currently under clinical evaluation. The implementation of RNA-based poly-neoepitope against a spectrum of melanoma mutations [5,6], gastrointestinal cancers [5,7], and triple-negative breast cancer [8] has been shown to activate neoepitope-specific $CD4^+$ and $CD8^+$ T cells, significantly reduce the metastatic events, and increase the progression-free survival. The Moderna vaccine mRNA-4157 (ClinicalTrials.gov identifier NCT03897881) [9,10] and BioNTech vaccine BNT122 (ClinicalTrials.gov identifier NCT04486378) [9,11,12] are currently undergoing phase II clinical trials for melanoma and high-risk colorectal cancer, respectively. This personalized approach holds strong potential for improving clinical outcomes in cancer treatment.

During the early development of mRNA therapeutics, strong antiviral responses induced by the IVT-mRNA were identified as a major obstacle to clinical use, as these responses can cause translational inhibition or even cell death in severe cases. To address this issue, strategies such as adding a 5′ cap structure [13,14], 3′ poly(A) tail [15,16], modifying uridine nucleotides [17,18], and removing double-stranded RNA (dsRNA) contaminant [19,20] have been applied. With these improvements, the chemically modified and purified IVT-mRNA has become suitable for clinical use. However, another challenge remains: IVT-mRNA is highly susceptible to enzymatic degradation in the extracellular environment. Therefore, its therapeutic application requires a suitable drug delivery system (DDS) that can protect mRNA in vivo and enable efficient cytoplasmic delivery.

Nanoformulations, such as polymer-based vectors [21,22] and lipid-based vectors [23,24], have emerged as promising platforms for mRNA delivery, providing advantages to address the limitations of naked mRNA. The lipid-based vectors, especially the lipid nanoparticles (LNPs), have been extensively studied for vaccine development. The approval of LNP-based mRNA vaccines (mRNA–LNPs) against severe acute respiratory syndrome coronavirus 2 (SARS-CoV-2) by Moderna (Spikevax®) [25,26] and Pfizer/BioNTech (Comirnaty®) [27,28] highlighted the versatility of the LNPs as an mRNA carrier. In cancer therapy, mRNA–LNP cancer vaccines have also shown remarkable promise in recent clinical studies. Notably, Moderna (mRNA-4157/V940) and BioNTech (autogene cevumeran) personalized neoantigen mRNA–LNP vaccine significantly reduced recurrence or mortality risk in melanoma [10] and pancreatic cancer [12], respectively. These findings underscore the clinical potential of mRNA–LNP vaccines in oncology.

It has been increasingly recognized that the LNPs, which are mainly composed of ionizable lipids, play dual roles in RNA vaccines: (1) delivering mRNA into the cytoplasm by overcoming the endosomal barrier and (2) stimulating the innate immune system as adjuvants [29–31]. The extent of these functions depends on the chemical structures of the ionizable lipids [32–34]. To maximize the potency of mRNA vaccines, one effective approach is to design hybrid particles that combine two or more different ionizable lipids, each optimized for a specific function. In previous studies, we developed disulfide-cleavable and pH-activated lipid-like materials (ssPalm). Modification of the hydrophobic scaffolds in ssPalm confers distinct physiological properties to the LNPs. Incorporation of a self-degradable phenyl oleate moiety enhances intracellular mRNA release and transfection activity (ssPalmO-Phe; SS-OP) [35,36], whereas ssPalm derivatives containing vitamin E scaffolds (ssPalmE; SS-EC) stimulate the type I interferon pathway [34].

In this study, we developed LNPs that combine the ionizable lipids ssPalmO-Phe (phenyl oleate) and ssPalmE (vitamin E), hereafter referred to as $LNP_{OP/EC}$, for mRNA cancer vaccine applications. We evaluated the ability of $LNP_{OP/EC}$ to induce immune and antitumor responses. E.G7-OVA cells expressing ovalbumin (OVA) were used as a model cancer antigen for optimization, followed by evaluation in a murine gastric cancer model (YTN16 cells) expressing three neoepitopes: mCdt1, mScarb2, and mZfp106 [37]. These experiments were conducted to evaluate the potential of $LNP_{OP/EC}$ as a platform for mRNA-based cancer vaccination.

2. Materials and methods

2.1. Animals

C57BL/6 J mice (C57BL/6JJmsSlc, female, 6–8 weeks) were purchased from Japan SLC, Inc. (Shizuoka, Japan). The animals were maintained under a 12 h light/12 h dark cycle. Protocols for the animal experiments were reviewed and approved by the Chiba University Animal Care Committee and Tohoku University Animal Care Committee following the "Guide for Care and Use of Laboratory Animals" (approval numbers: No. 4–175,492 (Chiba University), No. 2021–011-04 (Tohoku University), and No. ID: KAME-2024-006 (Kindai University)).

2.2. Materials

A detailed list of supplier information, including item numbers of all reagents used in this study, is provided in Supplementary Materials (Table S1). The ssPalmO-Phe (Product# COATSOME® SS-OP), ssPalmE (Product# COATSOME® SS-EC), 1,2-Dioleoyl-*sn*-glycero-3-phosphocholine (DOPC, Product# COATSOME® MC-8181), and (1,2-Dimyristoyl-rac-glycero-3-methoxypolyethylene glycol) 2000 (DMG-PEG_{2000}, Product# SUNBRIGHT® GM-020) were supplied by NOF CORPORATION (Tokyo, Japan). Cholesterol was purchased from Sigma-Aldrich (St. Louis, MO, USA). The mRNA encoding firefly luciferase (Luc) or ovalbumin (OVA) was prepared by in vitro transcription, as described in the following section. The Quant-IT™ RiboGreen® RNA reagent was purchased from Thermo Fisher Scientific (Waltham, MA, USA). All other reagents and chemicals were commercially available and used as received without further purification.

2.3. In vitro mRNA transcription (IVT-mRNA)

The pT7 vector was used as a coding template for luciferase (Luc) and ovalbumin (OVA). The pT7-Luc-UTR or pT7-OVA-UTR plasmid DNAs were linearized with the restriction enzyme *Asc*I (#R0558S, New England Biolabs, Ipswich, MA, USA). After phenol-chloroform extraction and ethanol precipitation, the linearized pDNA was transcribed into mRNA with a MEGAscript™ T7 Transcription Kit (#AM1334, Invitrogen, Waltham, MA, USA) according to the manufacturer's instructions. Uridine residues were substituted with N1-methylpseudouridine-5′-triphosphate (#N-1081-5, TriLink Biotechnologies, San Diego, CA, USA). The double-stranded RNA (dsRNA) contaminant was removed as described previously [19]. The 5′ cap structure and 3′ poly(A) tail were attached using ScriptCap™ Cap 1 Capping System (#C-SCCS1710, CELLSCRIPT, Madison, WI, USA) and Poly(A) Tailing Kit (#AM1350, Invitrogen, Waltham, MA, USA), respectively, following the manufacturer's instructions. The mRNA was dissolved in UltraPure™ DNase/RNase-Free Distilled Water (DDW) (#10977–023, Invitrogen, Waltham, MA, USA) and stored at −80 °C. The concentrations of linearized pDNA and transcribed mRNA were measured with a microvolume UV–Vis spectrometer (NanoDrop™ One,

Thermo Fisher Scientific, Waltham, MA, USA).

2.4. Neoantigens' mRNA preparation and purification

The mRNA, designed as a tandem minigene encoding three neoantigens (neoAgs) identified from the murine gastric cancer YTN16 cell line, was generated by in vitro transcription, following established procedures [38]. The neoAg-coding DNA fragment was synthesized using the GeneArt Strings DNA fragment synthesis service (Thermo Fisher Scientific, Waltham, MA, USA) and inserted into a plasmid DNA (pDNA) backbone containing 5′- and 3′-untranslated region (UTR) sequences. To obtain the transcription template, PCR amplification was performed using the neoAg-encoding pDNA as the template, PrimeSTAR MAX DNA polymerase (#R045A, Takara Bio, Shiga, Japan), a forward primer harboring the T7 promoter sequence, and a reverse primer carrying a 120-mer poly(T) tail. In vitro transcription was subsequently performed using either the MEGAscript T7 Transcription Kit (#AM1334, Invitrogen, Waltham, MA, USA) or the Takara IVTpro T7 mRNA Synthesis Kit (#6144, Takara Bio, Kusatsu, Shiga, Japan). Uridine residues were substituted with N1-methylpseudouridine-5′-triphosphate (#N-1081-5, TriLink Biotechnologies, San Diego, CA, USA). Co-transcriptional capping was achieved with CleanCap® Reagent AG (#N-7113, TriLink Biotechnologies, San Diego, CA, USA). Following transcription, the mRNA was purified using RNAClean XP (#A63987, Beckman Coulter Inc., Brea, CA, USA) and subsequently dephosphorylated with Quick CIP (#M0525S, New England Biolabs, Ipswich, MA, USA). The dephosphorylated mRNA was further purified using an RNeasy Mini Kit (#74104, Qiagen K.K., Tokyo, Japan). The concentration of the purified mRNA was quantified with a Nanodrop ONE spectrophotometer (Thermo Fisher Scientific, Waltham, MA, USA), and the transcript size was verified using an Agilent 2100 Bioanalyzer together with the RNA 6000 Nano Kit (Agilent Technologies Japan Ltd., Tokyo, Japan).

2.5. Preparation of mRNA–LNP

The ssPalm materials were synthesized according to previously reported methods [36,39]. A stock solution of 10 mM ssPalmO-Phe (SS-OP), 5 mM ssPalmE (SS-EC), 10 mM 1,2-Dioleoyl-*sn*-glycero-3-phosphocholine (DOPC), 10 mM cholesterol, and 2 mM (1,2-Dimyristoyl-rac-glycero-3-methoxypolyethylene glycol) 2000 (DMG-PEG_{2000}) was prepared in ethanol. Before use, the lipid stocks were warmed to 32 °C for 10 min to fully dissolve any precipitated lipids. These lipid stocks were then mixed to prepare a lipid mixture with a composition of ssPalmO-Phe/ssPalmE/DOPC/cholesterol = 32.5/20/7.5/40 with additional DMG-PEG_{2000} (1.5 mol% of total lipid) [36,40]. The amount of SS-EC was adjusted depending on the experiment by increasing or decreasing the SS-OP proportion while maintaining the total lipid percentage. The ratio of lipid to mRNA (lipid/mRNA, nmol/μg) was set to 33, 100, or 200 nmol/μg according to the experimental conditions. The lipid mixture was prepared at a concentration of 4.0 mM. The mRNA encoding luciferase or OVA was diluted in 20 mM malic acid buffer (30 mM NaCl, pH 3.0) to a concentration of 0.0067 μg/μL. The lipid mixture in ethanol and the mRNA solution were loaded to their respective syringes into NanoAssemblr device (Precision Nanosystems, Vancouver, Canada) with a flow rate of 4.0 mL/min and flow rate ratio (buffer: lipid) of 3: 1. The resulting suspension of LNPs in the ethanol/malic acid mixture was diluted with 20 mM MES buffer (pH 6.5) for at least 4-fold and transferred into Amicon Ultra-4-100 K Centrifugal Units (#UFC810096, #UFC910096, Merck, Rahway, NJ, USA). Centrifugation (1000 ×*g*, room temperature (RT)) was done to concentrate the LNPs suspension. The resulting LNPs retained in the upper cassette were re-diluted with the D-PBS(−) for at least 10-fold and centrifuged again (1000 ×*g*, RT). This buffer-exchange step was repeated twice. The LNP suspension was collected and diluted to the desired volume with D-PBS (−). The resulting mRNA–LNPs were then analyzed for their particle properties before being used in experiments.

2.6. Characterization of mRNA–LNPs

The particle size, polydispersity index (PdI), and zeta-potential of the LNPs were measured by dynamic light scattering (Zetasizer Nano ZS, Malvern Panalytical, Malvern, UK). The recovery ratio and encapsulation efficiency of the mRNA were evaluated with the RiboGreen® assay. The Quant-iT™ RiboGreen® RNA reagent (#R11491, Invitrogen, Waltham, MA, USA) was diluted 200-fold in D-PBS(−) with or without 0.4 % (*v/v*) TritonX-100 (#168–11805, FUJIFILM Wako Pure Chemical Corporation, Tokyo, Japan), hereafter referred to as Triton [+] and Triton [−], respectively. The mRNA–LNPs corresponding to 50 ng of mRNA in 50 μL of D-PBS(−) were prepared in duplicate and mixed with an equal volume of the Triton [+] and Triton [−] solution in a 96-well black microplate. A calibration curve was prepared by sequential dilution from 0 to 2000 ng/mL of mRNA. The plate was incubated in a shaking incubator for 5 min at 500 rpm. Fluorescence intensities were analyzed with a plate reader (Infinite M200 PRO, TECAN, Männedorf, Switzerland) set with emission and excitation wavelengths of 484 nm and 535 nm, respectively. The recovery ratio was calculated from the total mRNA (quantified by Triton [+] addition) relative to the input of mRNA concentration (based on a standard curve). The encapsulation efficiency was calculated as the ratio of the total mRNA concentration (Triton [+]) to the non-encapsulated mRNA concentration (Triton [−]).

2.7. In vivo cytotoxic T lymphocyte (CTL) assay

The in vivo CTL assay was performed as described previously [41,42]. The mRNA(OVA)–LNPs in D-PBS(−) were injected subcutaneously (back of neck) to C57BL/6 J mice at a dose equivalent to 0.05 μg of mRNA under anesthesia. Seven days after LNP immunization, spleens were collected from untreated (NT) mice into a dish containing RPMI-1640 medium (#R8758, Sigma-Aldrich, St. Louis, MO, USA) supplemented with 10 % (*v/v*) FCS (#SH30910.03, Hyclone, Logan, UT, USA), 50 μM of 2-mercaptoethanol (#21985023, Thermo Fisher Scientific, Waltham, MA, USA), 10 mM of HEPES buffer (#17557–94, nacalai tesque, Kyoto, Japan), 1 mM of sodium pyruvate (#06977–34, nacalai tesque, Kyoto, Japan), and 100 U/mL of penicillin/streptomycin (#26253–84, nacalai tesque, Kyoto, Japan). The splenocytes suspension was filtered through a 40 μm cell strainer and resuspended in Red Blood Cell Lysing Buffer (#R7757-100ML, Sigma-Aldrich, St. Louis, MO, USA). After washing, the cells were resuspended in fresh medium and divided equally into two suspensions: $CFSE^{high}$- and $CFSE^{low}$-labeled. Each cell suspension was adjusted to a concentration of 1.0×10^7 cells/mL. The OVA $H\text{-}2K^b$ cytotoxic T-lymphocyte epitope peptide (SIINFEKL, $OVA_{257–264}$) in DMSO was added to the $CFSE^{high}$-labeled cells (1/400 of the suspension volume). Both cell suspensions were incubated at 37 °C with 5 % CO_2 for 1 h. Each cell suspension was then adjusted to a concentration of 3.0×10^7 cells/mL in D-PBS(−). $CFSE^{high}$ (5.0 μM) and $CFSE^{low}$ (0.5 μM) (Cellstain CFSE, #C375, Dojindo Laboratories, Kumamoto, Japan) were added to their respective suspensions and incubated in a 37 °C water bath for 10 min under light-shielding conditions. After repeated washing with fresh medium and D-PBS(−), both suspensions were adjusted to a concentration of 5.0×10^7 cells/mL in D-PBS(−). The $CFSE^{high}$- and $CFSE^{low}$-labeled splenocytes were mixed at a 1:1 ratio and intravenously administered into the immunized mice. Twenty hours after administration, the spleens were collected from the immunized mice, and the splenocytes were suspended as single-cell suspensions in FACS buffer (0.5 % Bovine Serum Albumin (#01860–07, nacalai tesque, Kyoto, Japan) and 0.1 % NaN_3 (#194–01275, FUJIFILM Wako Pure Chemical Corporation, Tokyo, Japan) in D-PBS(−)). The numbers of CFSE-labeled cells ($CFSE^{high}$ and $CFSE^{low}$) were quantified using a flow cytometer (NovoCyte Flow Cytometer, Agilent, Santa Clara, CA, USA). CTL activity was determined by the degree of target cell lysis, calculated as the ratio of the number of

$CFSE^{high}$- to $CFSE^{low}$-labeled cells.

2.8. Cytokine IL-6 quantification

The quantification of cytokine IL-6 was performed as described previously [34]. Briefly, C57BL/6 J mice were subcutaneously injected with empty $LNP_{OP/EC}$ or empty $LNP_{ssPalmO\text{-}Phe}$ at a lipid dose equal to 200 nmol. Blood samples were collected at 6, 12, 18, 24, 30, 36, 42, and 48 h post-injection, and the serum was stored at −80 °C. Serum IL-6 cytokine levels were measured using Mouse IL-6 Quantikine ELISA Kit (#M6000B, R&D Systems, Minneapolis, MN, USA) following the manufacturer's instructions. For cytokine IL-6 quantification in skin tissue, 1.5 cm^2 skin samples were collected from the injection site and homogenized with ProcartaPlex™ Cell Lysis Buffer (#EPX-99999-000, Invitrogen, Waltham, MA, USA) using a micro smasher (TOMY SEIKO CO., LTD., Tokyo, Japan). The protein concentration of the homogenate was adjusted to 5 mg/mL using the BCA Protein Assay Kit (#T9300A, TaKaRa, Shiga, Japan). The cytokine IL-6 levels were measured using Mouse IL-6 ELISA (#ELM-IL6-CL-1, RayBiotech, Norcross, GA, USA).

2.9. Evaluation of in vivo gene expression efficiency (IVIS imaging)

The mRNA(Luc)–LNPs in D-PBS(−) were administered subcutaneously (back of neck) to C57BL/6 J mice at a dose equivalent to 1.0 μg of mRNA, under anesthesia. The neck region of the mice was shaved in advance. Six hours after administration, D-luciferin potassium (#126–05116, FUJIFILM Wako Pure Chemical Corporation, Tokyo, Japan) in D-PBS(−) (3 mg/200 μL/mouse) was administered intraperitoneally. After 30 min, luminescence intensities were measured with an In Vivo Imaging System (IVIS® Lumina II, Caliper Life Sciences, Waltham, MA, USA).

2.10. E.G7-OVA cell culture

E.G7-OVA cells, a murine lymphoma cell line derived from EL4-expressing OVA, were purchased from the American Type Culture Collection (Manassas, VA, USA). E.G7-OVA cells were cultured in RPMI-1640 medium (#R8758, Sigma-Aldrich, St. Louis, MO, USA) supplemented with 10 % (*v/v*) FCS (#SH30910.03, Hyclone, Logan, UT, USA), 50 μM of 2-mercaptoethanol (#21985023, Thermo Fisher Scientific, Waltham, MA, USA), 10 mM of HEPES buffer (#17557–94, nacalai tesque, Kyoto, Japan), 1 mM of sodium pyruvate (#06977–34, nacalai tesque, Kyoto, Japan), 400 μg/mL of G418 Sulfate (#074–05963, FUJIFILM Wako Pure Chemical Corporation, Tokyo, Japan), and 100 U/mL of penicillin/streptomycin (#26253–84, nacalai tesque, Kyoto, Japan). The cells were passaged every 2 days by transferring them into new dishes with fresh medium. The cells were used for experiments after the third passage [41,42].

2.11. Therapeutic anti-tumor response against E.G7-OVA

E.G7-OVA cells (8.0×10^5 cells/40 μL) suspended in D-PBS(−) were inoculated subcutaneously on the left flank of mice under anesthetized conditions. After tumors reached ≥100 mm^3 in volume (approximately 7–9 days), the mice were injected subcutaneously (back of neck) with mRNA(OVA)–LNPs at a dose equivalent to 0.5 μg of mRNA in D-PBS(−). Tumor sizes were measured every 3 days and calculated using the formula: {long axis} × $\{short\ axis\}^2 \times 0.52$ [41,42]. The endpoint of tumor measurement was set at 1000 mm^3.

2.12. Evaluation of neoantigen-specific T cell induction by neoantigen mRNA–$LNP_{OP/EC}$

C57BL/6 J mice were subcutaneously administered with 5.0 μg of mRNA(neoAg)–LNP or mRNA(Luc)–LNP vaccine twice (primary and booster) at 14-day intervals. Two weeks after the booster administration, spleens were harvested for MHC class I dimer assays and intracellular cytokine staining.

For MHC class I dimer preparation, 0.375 μg of each peptide (H-$2K^b$-mCdt1: KTVYPMSYRF, H-$2K^b$-OVA: SIINFEKL, H-$2D^b$-mScarb2: TSVINTTLV, H-$2D^b$-mZfp106: TSPRNSTVL, and H-$2D^b$-hgp100: KVPRNQDWL) was incubated with 0.5 μg of either DimerX I: Recombinant Soluble Dimeric Mouse H-$2K^b$ (#550750, BD Biosciences, Franklin Lakes, NJ, USA) or DimerX I: Recombinant Soluble Dimeric Mouse H-$2D^b$ (#551323, BD Biosciences, Franklin Lakes, NJ, USA) at 37 °C overnight. The peptide-loaded MHC class I dimers were then mixed with 0.5 μg of PE-conjugated anti-mouse IgG1 monoclonal antibody (clone RMG1–1, #406608, BioLegend, San Diego, CA, USA) and incubated for 60 min at room temperature, followed by a 30-min incubation with purified mouse IgG1 isotype control monoclonal antibody (clone MOPC-21, #400102, BioLegend, San Diego, CA, USA). The splenocytes were stained with the Zombie Aqua Fixable Viability Kit (#423102, BioLegend, San Diego, CA, USA) to exclude dead cells, followed by Fc receptor blocking using anti-CD16/32 antibody (clone 2.4G2, #BE0307, BioXCell, Lebanon, NH, USA). The cells were stained with the MHC class I dimers for 2 h at 4 °C, followed by staining with monoclonal antibodies (mAbs) for cell-surface antigens.

For intracellular cytokine staining, splenocytes (1×10^6) were cultured with the indicated peptides (1 μg/mL) or YTN16 cells (1×10^5) in the presence of brefeldin A (10 μg/mL, #B7651, Sigma-Aldrich, St. Louis, MO, USA) for 4 h. Dead cells were stained using the Zombie Aqua Fixable Viability Kit (#423102, BioLegend, San Diego, CA, USA), followed by Fc receptor blocking with anti-CD16/32 antibody (clone 2.4G2, #BE0307, BioXCell, Lebanon, NH, USA). Cells were then stained with mAbs for cell-surface antigens. After fixation with Fixation Buffer (#420801, BioLegend, San Diego, CA, USA) and permeabilization with Intracellular Staining Perm Wash Buffer (#421002, BioLegend, San Diego, CA, USA), cells were stained intracellularly with mAbs for IFN-γ (#505826, BioLegend, San Diego, CA, USA) and TNF-α (#506306, BioLegend, San Diego, CA, USA).

To expand neoantigen-specific T cells, splenocytes were cultured with the RMA cells pulsed with mCdt1, mScarb2, and mZfp106 peptides (1 μg/mL) for 6 days. Cultured cells were harvested and stimulated with the peptides or YTN16 cells in the presence of brefeldin A for 4 h, followed by intracellular cytokine staining as described above. The stained cells were analyzed using a CytoFLEX flow cytometer (Beckman Coulter, Brea, CA, USA). Data were processed and analyzed using FlowJo software (BD Biosciences, Franklin Lakes, NJ, USA).

2.13. Evaluation of mRNA(OVA) vaccine-induced immune responses in E.G7-OVA tumor model

Mice were subcutaneously inoculated with E.G7-OVA cells (8.0×10^5 cells/40 μL) on day 0. On day 7, mice were administered mRNA (OVA)–LNPs at a dose equivalent to 0.5 μg mRNA. Tumor size was measured every 2–3 days using calipers. On day 14, tumors were harvested and digested with 0.2 % collagenase (#032–22364, FUJIFILM Wako Pure Chemical Corporation, Tokyo, Japan) and 2 kU/mL DNase I (D4263, Sigma-Aldrich, St. Louis, MO, USA) for 40 min at 37 °C. The digested tissues were passed through a 70 μm cell strainer to obtain a single-cell suspension. Cells were stained with Zombie Aqua Fixable Viability Kit (#423102, BioLegend, San Diego, CA, USA) for 30 min, followed by staining with the OVA MHC class I dimer complex for 2 h and then with antibodies for cell-surface antigens for 30 min. Subsequently, cells were fixed and permeabilized with Fixation buffer (#420801, BioLegend, San Diego, CA, USA) and permeabilized with Intracellular Staining Perm Wash Buffer (#421002, BioLegend, San Diego, CA, USA) and then stained with APC anti-Granzyme B antibody (#372204, BioLegend, San Diego, CA, USA).

For intracellular cytokine staining, the cells were stimulated with OVA peptide (SIINFEKL) or E.G7-OVA cells in the presence of brefeldin A (10 μg/mL, #B7651, Sigma-Aldrich, St. Louis, MO, USA) for 4 h. Cells

were stained with Zombie Aqua Fixable Viability Kit (#423102, BioLegend, San Diego, CA, USA) for 30 min, followed by staining with antibodies for cell-surface antigens for 30 min. Cells were then fixed and permeabilized with Fixation buffer (#420801, BioLegend, San Diego, CA, USA) and permeabilized with Intracellular Staining Perm Wash Buffer (#421002, BioLegend, San Diego, CA, USA) and subsequently stained with PE/Cyanine7 anti-IFN-γ antibody (#505826, BioLegend, San Diego, CA, USA). The stained cells were analyzed using the CytoFLEX S flow cytometer (Beckman Coulter, Brea, CA, USA), and data were analyzed using FlowJo software (BD Biosciences, Franklin Lakes, NJ, USA).

2.14. Evaluation of neoantigen-specific $CD8^+$ T cells in the YTN16 tumor model

Mice were subcutaneously inoculated with YTN16 (5×10^6 cells/100 μL) cells on day 0. On days 7 and 14, mice were administered with mRNA(Luc)–LNPs or mRNA (neoAg)–LNPs at a dose of 5.0 μg mRNA. Tumor size was measured every 2–3 days using calipers. On day 18, tumors were harvested and digested with 0.2 % collagenase (#032–22364, FUJIFILM Wako Pure Chemical Corporation, Tokyo, Japan) and 2 kU/mL DNase I (#D4263, Sigma-Aldrich, St. Louis, MO, USA) for 40 min at 37 °C. The digested tissues were passed through a 70 μm cell strainer to obtain a single-cell suspension. Cells were stained with Zombie Aqua Fixable Viability Kit (#423102, BioLegend, San Diego, CA, USA) for 30 min, followed by staining with the MHC class I dimer complexes (H-$2K^b$-mCdt1, H-$2D^b$-mScarb2, H-$2D^b$-mZfp106) for 2 h, and then with antibodies for cell-surface antigens for 30 min. Stained cells were acquired on a CytoFLEX S flow cytometer (Beckman Coulter, Brea, CA, USA), and data were analyzed using FlowJo software (BD Biosciences, Franklin Lakes, NJ, USA).

2.15. Statistics

One-way ANOVA (followed by Bonferroni or Student–Newman–Keuls (SNK) tests) and Mann–Whitney *U* test were employed for multiple comparisons, while a two-tailed *t*-test was used for the comparisons between two groups. The survival rate of tumor-bearing mice in antitumor response evaluation was determined by Kaplan-Meier analysis. Data analyses were performed using Excel (Microsoft, Redmond, WA, USA) with an add-in software Statcel4 (ISBN: 4434211625). A *P* value of <0.05 (*) and < 0.01 (**) was considered statistically significant. Details of the statistical analyses are provided in the figure captions.

3. Results

3.1. ssPalmE content influences cellular immunity and gene expression of mRNA–LNP

Preliminary experiments showed that $LNP_{ssPalmE}$ exhibited significantly higher CTL activity (Fig. S1a), but approximately 30-fold lower gene expression compared with $LNP_{ssPalmO\text{-}Phe}$ (Fig. S1b). This significant activation of cellular immunity despite the low level of antigen expression is attributed to the adjuvant activity of the vitamin E moiety. As shown in previous reports [34], empty-LNPs containing ssPalmE alone exhibit significant adjuvant activity when co-administered with protein antigens, whereas other ssPalm molecules with fatty acid scaffolds do not. To maximize the immune-activating characteristics of ssPalmE, we aimed to confer high gene expression capacity for $LNP_{ssPalmE}$. The $LNP_{OP/EC}$ formulation was designed by combining ionizable lipids ssPalmO-Phe and ssPalmE (Fig. 1a). The LNPs also contained helper lipids such as 1,2-Dioleoyl-*sn*-glycero-3-phosphocholine (DOPC), cholesterol, and 1,2-Dimyristoyl-rac-glycero-3-methylpolyoxyethylene ($DMG\text{-}PEG_{2000}$) (Fig. 1a), to stabilize the LNP formulation. The $LNP_{OP/EC}$ was prepared with a composition of ssPalm (s)/DOPC/Chol = 52.5/7.5/40 (% total lipid) with an additional 1.5 % of $DMG\text{-}PEG_{2000}$ [36,40]. $LNP_{OP/EC}$ with different compositions, along with $LNP_{ssPalmO\text{-}Phe}$ (control) encapsulating mRNAs, were prepared using a microfluidic mixer (Fig. 1b). To optimize the ratio of ionizable lipids, the ssPalmE content was varied from 5 to 30 % while maintaining the total ionizable lipid fraction at 52.5 % of total lipid. Details of the $LNP_{OP/EC}$ compositions are summarized in Table 1. There were no substantial differences in particle properties between $LNP_{OP/EC}$ and $LNP_{ssPalmO\text{-}Phe}$, with average particle sizes of approximately 80–95 nm, an acceptable polydispersity index (PdI) (< 0.200), and slightly negative surface charge (−3 to −5 mV) due to the nucleic acid payload (Table 1). All LNP types demonstrated a high mRNA encapsulation efficiency (> 90 %) and similarly high recovery rates (> 90 %) (Table 1).

To evaluate the capability of $LNP_{OP/EC}$ to activate cell-mediated immunity, the CTL assay was performed using the model antigen ovalbumin. The CTL activity of mRNA(OVA)–$LNP_{OP/EC}$ increases in proportion to the ssPalmE content, with statistically significant differences observed from 20 % to 30 % ssPalmE compared with the control (Fig. 1c, Fig. S2, Fig. S3). CTL activity remained detectable for up to 2 months after a single subcutaneous administration of $LNP_{OP/EC(20\%)}$ (Fig. S4a–c). Although the CTL activity of $LNP_{OP/EC(20\%)}$ was comparable to that of $LNP_{ssPalmE}$ at 1 week and 1 month after administration, it became significantly higher at 2 months after administration (Fig. S4c). The production of antibodies against OVA was quantified by ELISA to evaluate the ability of $LNP_{OP/EC}$ to induce a humoral immune response; however, no clear dependence on ssPalmE content was observed among all $LNP_{OP/EC}$ formulations (Fig. S5a, b). These findings indicate that the vitamin E moiety in ssPalmE provides immune-activating properties that enhance the adjuvant effect of $LNP_{OP/EC}$, particularly in cell-mediated immunity.

In vivo gene expression was also evaluated to investigate the effect of vitamin E scaffolds on transfection efficiency. Gene expression was assessed in mice subcutaneously injected with mRNA(Luc)–$LNP_{OP/EC}$(s) at a dose equivalent to 1.0 μg of mRNA. Six hours post-injection, luciferin was administered, and luminescence intensities were measured using an In Vivo Imaging System (IVIS®) device. $LNP_{ssPalmO\text{-}Phe}$ and $LNP_{SM\text{-}102}$, prepared according to previous studies [43,44], served as controls. The findings indicated that as the ssPalmE content increased, gene expression of $LNP_{OP/EC}$ decreased (Fig. 1d, e). A significant reduction in gene expression was observed in $LNP_{OP/EC}$ formulations containing 20, 25, and 30 % of ssPalmE content, compared to $LNP_{ssPalmO\text{-}Phe}$ as a control.

3.2. Cytokine IL-6 production and toxicity evaluation

To further assess the properties of $LNP_{OP/EC}$ as a vaccine carrier, local (skin) and systemic (serum) levels of cytokine IL-6 were quantified as an indicator of innate immune activation. IL-6 production in the skin (Fig. 2a, b) and serum (Fig. 2c, d) increased proportionally with the ssPalmE content, a trend consistent with the results observed in the CTL assay (Fig. 1c). $LNP_{OP/EC(20\%)}$ was selected as a representative formulation to quantify cytokine IL-6 levels, which revealed transient IL-6 induction following LNP administration. IL-6 concentrations in the skin (Fig. 2b) and serum (Fig. 2d) increased rapidly, reaching their peak at 6 h post-injection, and then gradually declined to baseline level by 24 h. These findings suggest that although $LNP_{OP/EC}$ induces measurable innate immune activation, the effect is short-lived, thereby minimizing the risk of adverse side effects. Considering the enhanced CTL activity (Fig. 1c), increased IL-6 production (Fig. 2a-d), and reduced gene expression (Fig. 1d, e), an ssPalmE content of 20 % was selected for subsequent $LNP_{OP/EC}$ formulations to balance immune stimulation with delivery efficiency. Having established 20 % ssPalmE as the baseline composition, further optimization was conducted to adjust the ratios of phospholipid (DOPC, 7.5–22.5 %) and cholesterol (20–60 %) in $LNP_{OP/EC}$, while fixing the ssPalmE content at 20 % (Fig. S6a). The optimization was carried out by assessing the in vivo gene expression. The original

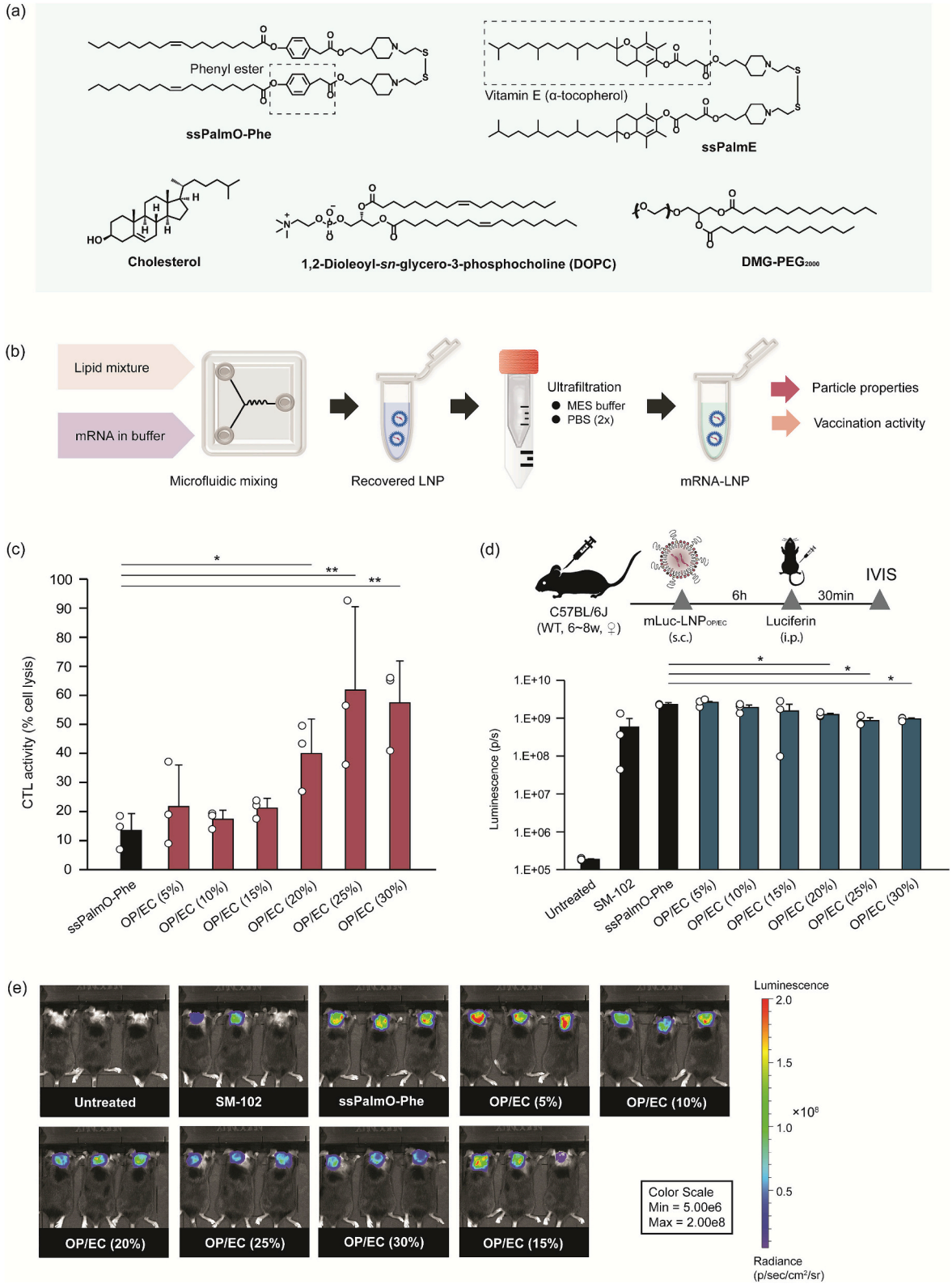

Fig. 1. Induction of immune responses and gene transfection activity of $LNP_{OP/EC}$.
(a) Chemical structures of the lipids used in this study. (b) Schematic illustration of LNP preparation. (c) CTL activity of $LNP_{OP/EC}$ with different compositions of ionizable lipid. CTL assay was conducted in C57BL/6 J mice following subcutaneous (s.c.) immunization of mRNA(OVA)–$LNP_{OP/EC}$ at a dose of 0.05 μg of mRNA. Spleens were collected, and the percentage of splenocytes lysis was quantified by flow cytometry. (d, e) Quantification and imaging results of mRNA(Luc)-LNPs in vivo gene expression. C57BL/6 J mice were injected (s.c.) with mRNA(Luc)–LNPs at a dose of 1.0 μg of mRNA. Six hours after administration, D-luciferin potassium (3 mg/200 μL/mouse) was administered intraperitoneally (i.p.), and the luminescence intensity was measured using an IVIS® device. Scatter plots represent individual values; bar graphs represent the mean with SD ($n = 3$); $^{**}p < 0.01$, $^{*}p < 0.05$ (one-way ANOVA followed by a Bonferroni test versus $LNP_{ssPalmO\text{-}Phe}$).

Table 1
Lipid composition and physicochemical properties of mRNA(OVA)-$LNP_{OP/EC}$.

LNP	Composition (mol%)					Size (nm)	PdI	ZP (mV)	Recovery (%)	Encaps. (%)
	ssPalmO-Phe	ssPalmE	DOPC	Chol	$DMG\text{-}PEG_{2000}$					
ssPalmO-Phe	52.5	0	7.5	40	1.5	92.5 ± 7.7	0.13 ± 0.007	−3.3 ± 0.5	98.4 ± 1.2	95.1 ± 2.4
OP/EC (5 %)	47.5	5	7.5	40	1.5	94.6 ± 3.7	0.12 ± 0.001	−4.1 ± 0.2	100.0 ± 3.7	95.6 ± 1.8
OP/EC (10 %)	42.5	10	7.5	40	1.5	84.6 ± 0.6	0.13 ± 0.032	−4.5 ± 0.3	100.0 ± 2.5	95.4 ± 1.9
OP/EC (15 %)	37.5	15	7.5	40	1.5	87.9 ± 1.4	0.13 ± 0.002	−4.7 ± 0.6	97.1 ± 2.7	96.7 ± 2.4
OP/EC (20 %)	32.5	20	7.5	40	1.5	85.9 ± 0.6	0.12 ± 0.056	−4.0 ± 0.6	99.2 ± 3.7	96.9 ± 1.6
OP/EC (25 %)	27.5	25	7.5	40	1.5	85.4 ± 1.5	0.14 ± 0.031	−4.3 ± 0.9	94.7 ± 3.4	97.5 ± 2.0
OP/EC (30 %)	22.5	30	7.5	40	1.5	83.9 ± 1.7	0.14 ± 0.020	−3.9 ± 0.4	100.0 ± 1.8	97.5 ± 2.6

Size, PdI, and ZP were measured with Zetasizer Nano ZS. Encapsulation efficiency was measured with the Ribogreen® assay. Mean ± SD ($n = 3$).

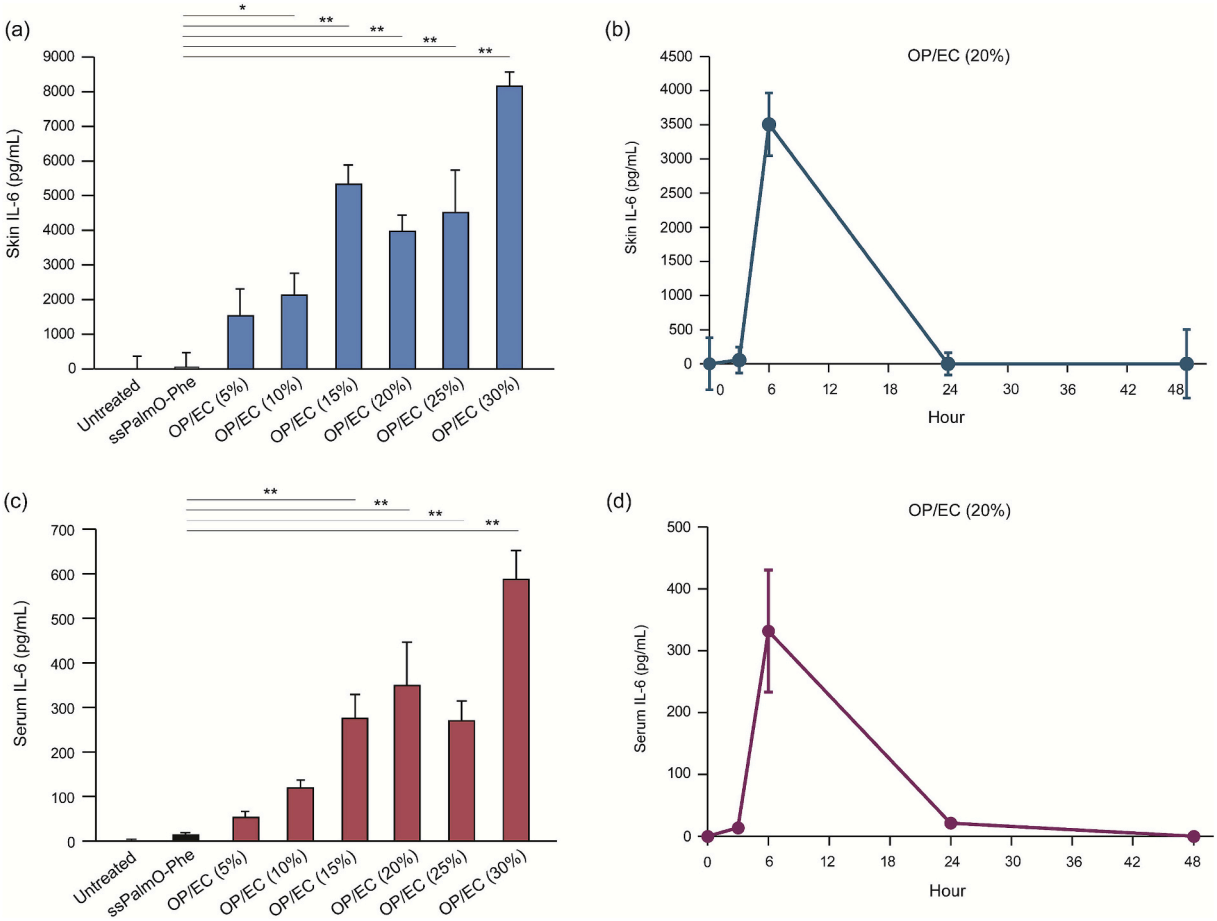

Fig. 2. Cytokine IL-6 production in serum and at the injection site.
IL-6 levels were quantified by ELISA following subcutaneous injection of empty LNPs at a lipid dose equal to 200 nmol. Serum and skin samples were collected at the indicated time points, and IL-6 levels were measured accordingly. (a) Serum IL-6 at 6 h post-injection. (b) Serum IL-6 was measured over a 0–48 h time course. (c) Skin (injection site) IL-6 at 6 h post-injection. (d) Skin IL-6 was measured over a 0–48 h time course. Bar graphs represent the mean with SD ($n = 3$); $^{**}p < 0.01$, $^{*}p < 0.05$ (Mann–Whitney U test).

composition of ssPalmO-Phe/ssPalmE/DOPC/Chol = 32.5/20/7.5/40 (% total lipid) yielded the highest gene expression (Fig. S6b, c), indicating that this formulation represents the optimal LNP composition for further studies.

The toxicity of $LNP_{OP/EC(20\%)}$ was also evaluated. Local cytotoxicity at the injection site was assessed by measuring the percentage of cell death in skin tissue following administration. The results demonstrated that $LNP_{OP/EC(20\%)}$ induced a rate of cell death comparable to that of $LNP_{ssPalmO\text{-}Phe}$ (Fig. S7a, b), indicating that the formulation does not cause excessive local tissue damage. In addition, systemic toxicity potentially arising from LNPs leaked into the bloodstream was examined by measuring serum alanine transaminase (ALT) and aspartate transaminase (AST) levels at 6 and 24 h post-administration, comparing $LNP_{OP/EC(20\%)}$ with untreated mice, $LNP_{ssPalmO\text{-}Phe}$, and $LNP_{ssPalmE}$ as controls. The results showed that ALT and AST levels in the $LNP_{OP/EC(20\%)}$ group remained comparable to those in the control groups (Fig. S7c, d). These results indicate that $LNP_{OP/EC(20\%)}$ does not induce significant hepatotoxicity even when LNPs enter the bloodstream, and is well tolerated both locally and systemically.

3.3. An optimal $LNP_{OP/EC}$ concentration is essential for maximizing immunostimulatory efficacy

Based on the initial evaluation of the $LNP_{OP/EC}$ formulation, $LNP_{OP/}$

$_{EC(20\%)}$ was selected for subsequent experiments. The next phase of optimization involved determining the lipid/mRNA (L/R; nmol/μg) ratio, which correlates with the lipid concentration in the mRNA–LNP formulation. Previous studies have shown that increasing the lipid concentration of administered LNPs tends to enhance the immune response, but also increases toxicity risks [45,46]. Three L/R ratios were selected for evaluation: 33, 100, and 200 nmol/μg. The 33 nmol/μg ratio corresponds to the LNP_{SM-102} dosage used in mice in a previous study [43], while the 200 nmol/μg ratio was based on the dosage used in gene therapy with $LNP_{ssPalmO-Phe}$ [36,40]. The 100 nmol/μg ratio was chosen as an intermediate value.

Cell-mediated immunity was assessed using a CTL assay. In these experiments, the mRNA dose was fixed to 0.05 μg while the lipid dose was adjusted according to the L/R ratio. It was revealed that $LNP_{OP/EC(20\%)}$ at an L/R ratio of 100 nmol/μg exhibited the highest CTL activity, followed by the 200 nmol/μg group, whereas the 33 nmol/μg group showed almost no CTL activity (Fig. 3a, Fig. S8). A different trend was observed in the antibody production evaluation. After the primary immunization, $LNP_{OP/EC}$ with an L/R ratio of 100 nmol/μg induced the highest antibody levels, followed by L/R 33 and 200 nmol/μg groups (Fig. 3b). However, post-booster immunization showed a shift, with the L/R ratios of 33 and 100 nmol/μg inducing comparable antibody levels, while the L/R 200 nmol/μg group showed the lowest antibody level (Fig. 3c). These findings indicate that optimizing the L/R ratio is critical to enhance the immunostimulatory properties of $LNP_{OP/EC}$ for effective mRNA vaccine delivery. Based on these results, $LNP_{OP/EC(20\%)}$ with an L/R ratio of 100 nmol/μg was selected for further studies because of its superior vaccine efficacy.

3.4. $LNP_{OP/EC(20\%)}$ promotes tumor regression and functional activation of $CD8^+$ T cells

To assess the effectiveness of $LNP_{OP/EC(20\%)}$ as an mRNA vaccine carrier, we evaluated its ability to induce therapeutic antitumor response against the E.G7-OVA tumor model. A single subcutaneous injection of $LNP_{OP/EC(20\%)}$ (L/R 100 nmol/μg) at a dose equivalent to 0.5 μg of mRNA(OVA) was administered on day 7 after the tumor inoculation to evaluate its long-term antitumor effect. Administration of $LNP_{OP/EC(20\%)}$ significantly suppressed the tumor growth (Fig. 4a). Survival analysis, using a tumor size of 1000 mm^3 as the endpoint, showed that all mice in the immunized group survived without dropout up to 25 days post–tumor inoculation (Fig. 4b).

To further characterize the immune response, tumor tissues were analyzed at an earlier time point. On day 7, the $LNP_{OP/EC(20\%)}$ was injected into the mice, and on day 14 post-tumor inoculation, the $LNP_{OP/EC(20\%)}$ group showed significant tumor growth suppression compared with the untreated control (Fig. S9a-c). Tumors were harvested and examined by flow cytometry to evaluate $CD8^+$ T cell activation. Although the proportion of $CD45^+$ cells was comparable between groups (Fig. 4c, Fig. S10), $CD8^+$ T cells were significantly increased in the mRNA(OVA)–$LNP_{OP/EC(20\%)}$-immunized group (Fig. 4d, Fig. S10). Moreover, the frequency of MHC class I (H-2Kb)–OVA dimer-positive $CD8^+$ T cells was significantly elevated within the tumors of the immunized group (Fig. 4e, Fig. S10). These results indicate that $LNP_{OP/EC(20\%)}$ vaccination effectively primes and expands OVA-specific $CD8^+$ T cells, enabling them to infiltrate the tumor microenvironment as tumor-infiltrating lymphocytes (TILs).

To assess the cytotoxic potential of these TILs, we evaluated Granzyme B expression in MHC class I (H-2Kb)–OVA dimer-positive $CD8^+$ T cells. Granzyme B is a key effector molecule released by activated $CD8^+$ T cells to induce apoptosis in target cells [47,48]. In the immunized group, more than half of the OVA-specific $CD8^+$ T cells expressed Granzyme B (Fig. 4f, Fig. S11), indicating that a substantial fraction of these TILs exhibited cytotoxic potential.

We further investigated their cytokine-producing capacity by measuring IFN-γ production upon antigen-specific stimulation. Single-cell suspensions from tumors were cultured for 4 h under three conditions: unstimulated, OVA peptide-stimulated, or E.G7-OVA cell-stimulated, followed by intracellular IFN-γ staining. $LNP_{OP/EC(20\%)}$ vaccination significantly increased the frequency of IFN-γ–producing $CD8^+$ T cells in response to both OVA peptide and E.G7-OVA stimulation, compared with cells from untreated control mice (Fig. 4g, h, Fig. S12). These findings demonstrate that $LNP_{OP/EC(20\%)}$ vaccination not only expands antigen-specific $CD8^+$ TILs but also provides them with

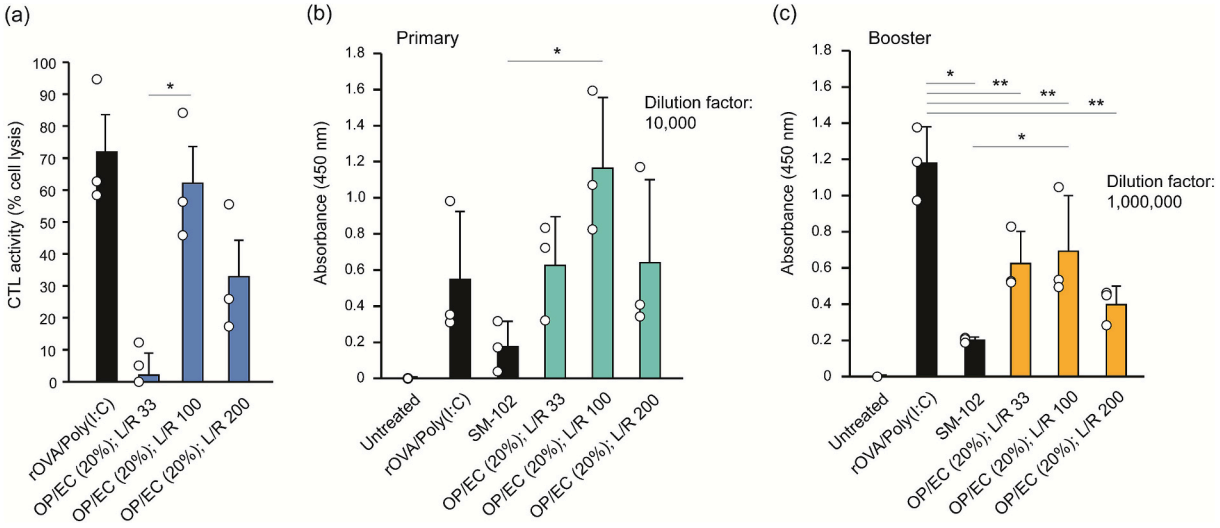

Fig. 3. Influence of lipid concentration on the CTL activity and antibody production of $LNP_{OP/EC}$.
(a) The mRNA(OVA)–$LNP_{OP/EC(20\%)}$ with different lipid concentrations (33, 100, and 200 nmol/μg) were evaluated for their immune activation by the CTL assay. A mixture of recombinant OVA protein (rOVA,10 μg) and Poly(I:C) (2 μg) was used as a control. C57BL/6 J mice were immunized (s.c.) with mRNA(OVA)–$LNP_{OP/EC(20\%)}$ equivalent to 0.05 μg of mRNA. Spleens were collected, and the percentage of splenocytes lysis was quantified by flow cytometry. (b) OVA-specific total IgG levels were measured after primary immunization and (c) after booster immunization of $LNP_{OP/EC(20\%)}$. C57BL/6 J mice were injected (s.c.) with mRNA(OVA)–$LNP_{OP/EC(20\%)}$ at a dose equivalent to 1.5 μg of mRNA, twice (primary and booster) at a 14-day interval. Blood serum was collected on day 14 following each administration, and anti-OVA total IgG levels were quantified by ELISA. Scatter plots represent individual values; bar graphs represent the mean with SD ($n = 3$); $^{**}p < 0.01$, $^{*}p < 0.05$ (one-way ANOVA followed by SNK test). Original scatter plots and gating strategies for flow cytometry analyses are provided in Supplementary Materials.

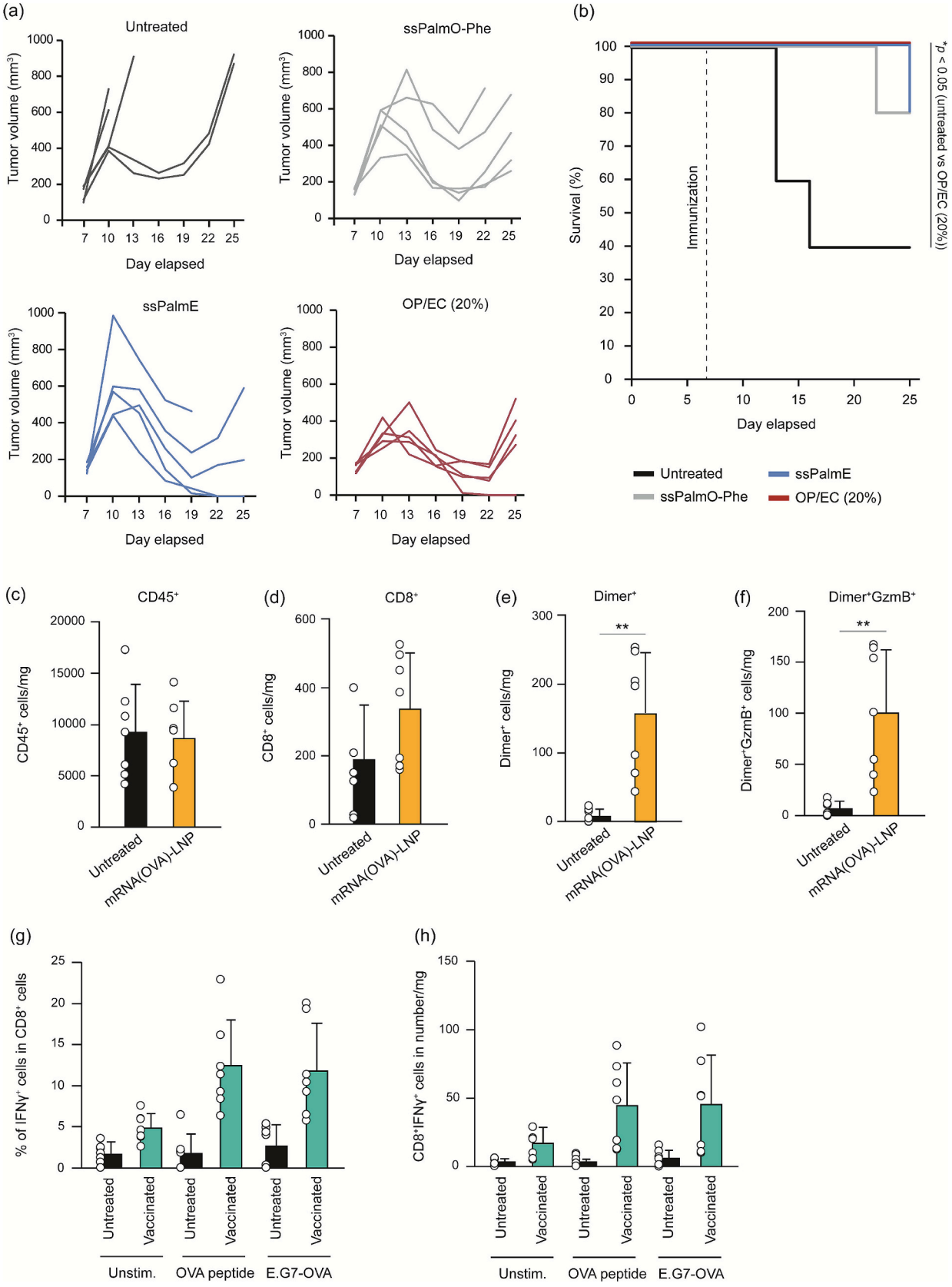

(caption on next page)

Fig. 4. Therapeutic antitumor response induced by $LNP_{OP/EC(20\%)}$.
The antitumor efficacy of $LNP_{OP/EC(20\%)}$ was evaluated in an E.G7-OVA tumor model. E.G7-OVA cells (8.0×10^5 cells/40 μL) were subcutaneously inoculated into the left flank of C57BL/6 J mice ($n = 5$). When tumors reached ≥100 mm^3, mice were administered a single subcutaneous injection of mRNA(OVA)–$LNP_{OP/EC(20\%)}$ at a dose equivalent to 0.5 μg of mRNA. Tumor volumes were measured every 3 days, and the experimental endpoint was defined as a tumor size of 1000 mm^3. (a) Individual tumor growth curves and (b) Kaplan–Meier survival analysis of tumor-bearing mice; significant differences were observed between untreated and $LNP_{OP/EC(20\%)}$ groups ($p < 0.05$). Flow cytometric analysis of tumor-derived immune cells on day 14: (c) $CD45^+$ cells, (d) $CD8^+$ T cells, and (e) MHC class I (H-2Kb)–OVA dimer-positive $CD8^+$ T cells. (f) Granzyme B expression in MHC class I (H-2Kb)–OVA dimer-positive $CD8^+$ T cells. (g, h) Functional analysis of tumor-derived $CD8^+$ T cells. Cells were cultured for 4 h under three conditions (unstimulated, OVA peptide-stimulated, or E.G7-OVA-stimulated), followed by intracellular IFN-γ staining. Scatter plots represent individual values; bar graphs represent the mean with SD ($n = 5$–7); $^{**}p < 0.01$, $^{*}p < 0.05$ (Mann-Whitney *U* test). Original dot plots and gating strategies for flow cytometry analyses are provided in Supplementary Materials.

functional capacity, including cytotoxic molecule expression and cytokine production, thereby driving the potent antitumor responses and prolonged survival observed in the E.G7-OVA tumor model.

3.5. T cell response against neoantigens

The capability of $LNP_{OP/EC(20\%)}$ to deliver neoantigen (neoAg) mRNAs encoding mCdt1, mScarb2, and mZfp106 was evaluated by administering mRNA(neoAg)–LNP $_{OP/EC(20\%)}$ to C57BL/6 mice twice, with a 14-day interval between doses. These neoantigens were originally identified from the murine gastric cancer cell line YTN16, which serves as a syngeneic tumor model for evaluating neoantigen-specific immune responses in C57BL/6 mice [37,38]. The population of antigen-specific T cells was analyzed by flow cytometry (Fig. S13). Following immunization, spleens were collected, and $CD8^+$ T cells were analyzed by flow cytometry to assess the induction of neoantigen-specific responses. Neoantigen-specific $CD8^+$ T cells, including mCdt1–H-$2K^b$–$dimer^+$, mScarb2–H-$2D^b$–$dimer^+$, and mZfp106–H-$2D^b$–$dimer^+$ cells, were detected in immunized mice (Fig. 5a-e, Fig. S14). Previous studies have shown that neoantigen-reactive $CD8^+$ T cells produce IFN-γ and TNF-α [37,49].

To further evaluate the induction of neoantigen-specific $CD8^+$ T cells, splenocytes were stimulated in vitro with mCdt1, mScarb2, and mZfp106 peptides, as well as with IFN-γ–treated YTN16 cells. IFN-γ production was detected in response to the three neoantigen peptides (Fig. 6a, Fig. S15). A similar trend was observed for TNF-α production (Fig. 6b, Fig. S16) and IFN-γ/TNF-α co-production (Fig. 6c, Fig. S17). Notably, these neoantigen-specific $CD8^+$ T cells also responded to YTN16 tumor cells, indicating that they recognized and reacted to endogenously expressed and naturally presented neoantigens.

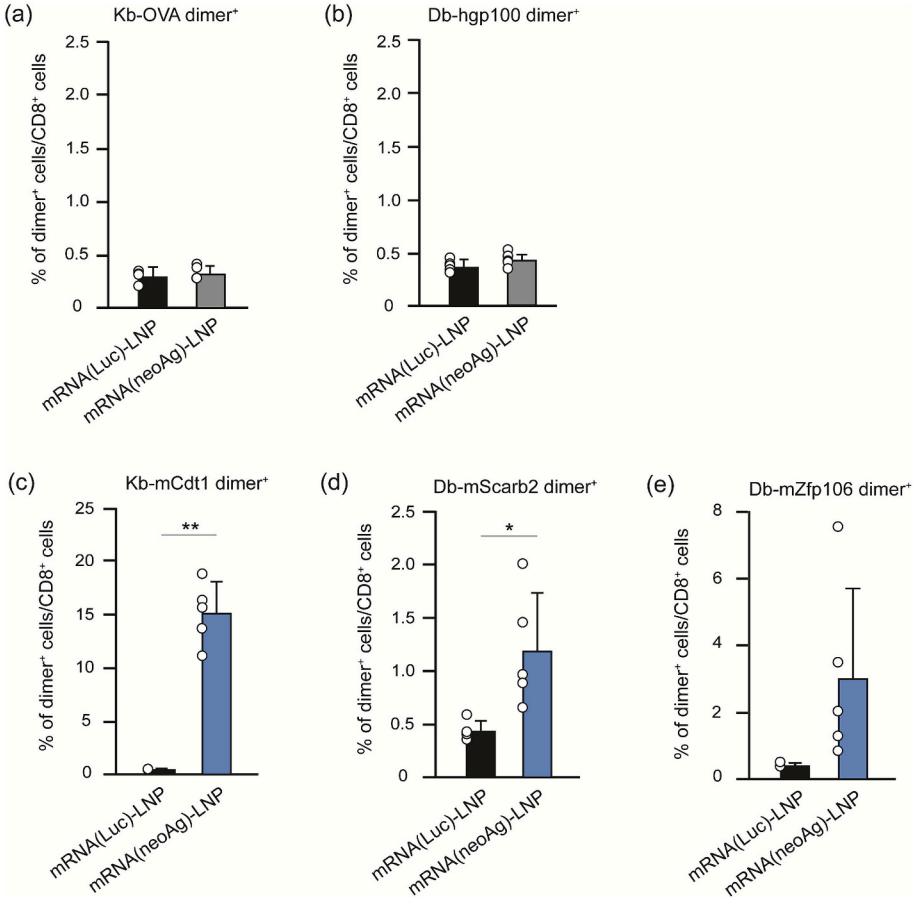

Fig. 5. Induction of neoantigen-specific T cells by $LNP_{OP/EC}$.
Mice were immunized with mRNA(neoAg)–LNP $_{OP/EC(20\%)}$ or mRNA(Luc)–LNP $_{OP/EC(20\%)}$ at a dose equivalent to 5.0 μg of mRNA, twice (primary and booster) at 14-day intervals. Two weeks after the booster immunization, spleens were collected, and neoantigen-specific T cells were evaluated using MHC class I dimers. Bar graphs show frequency of cells positive for (a) H-$2K^b$–OVA and (b) H-$2D^b$–hgp100, which served as negative controls, and for (c) H-$2K^b$–mCdt1, (d) H-$2D^b$–mScarb2, and (e) H-$2D^b$–mZfp106 dimers, which represent neoAg-specific responses. Scatter plots represent individual values; bar graphs represent the mean with SD ($n = 5$); $^{**}p < 0.01$, $^{*}p < 0.05$ (two-tailed *t*-test). Original dot plots and gating strategies for flow cytometry analyses are provided in Supplementary Materials.

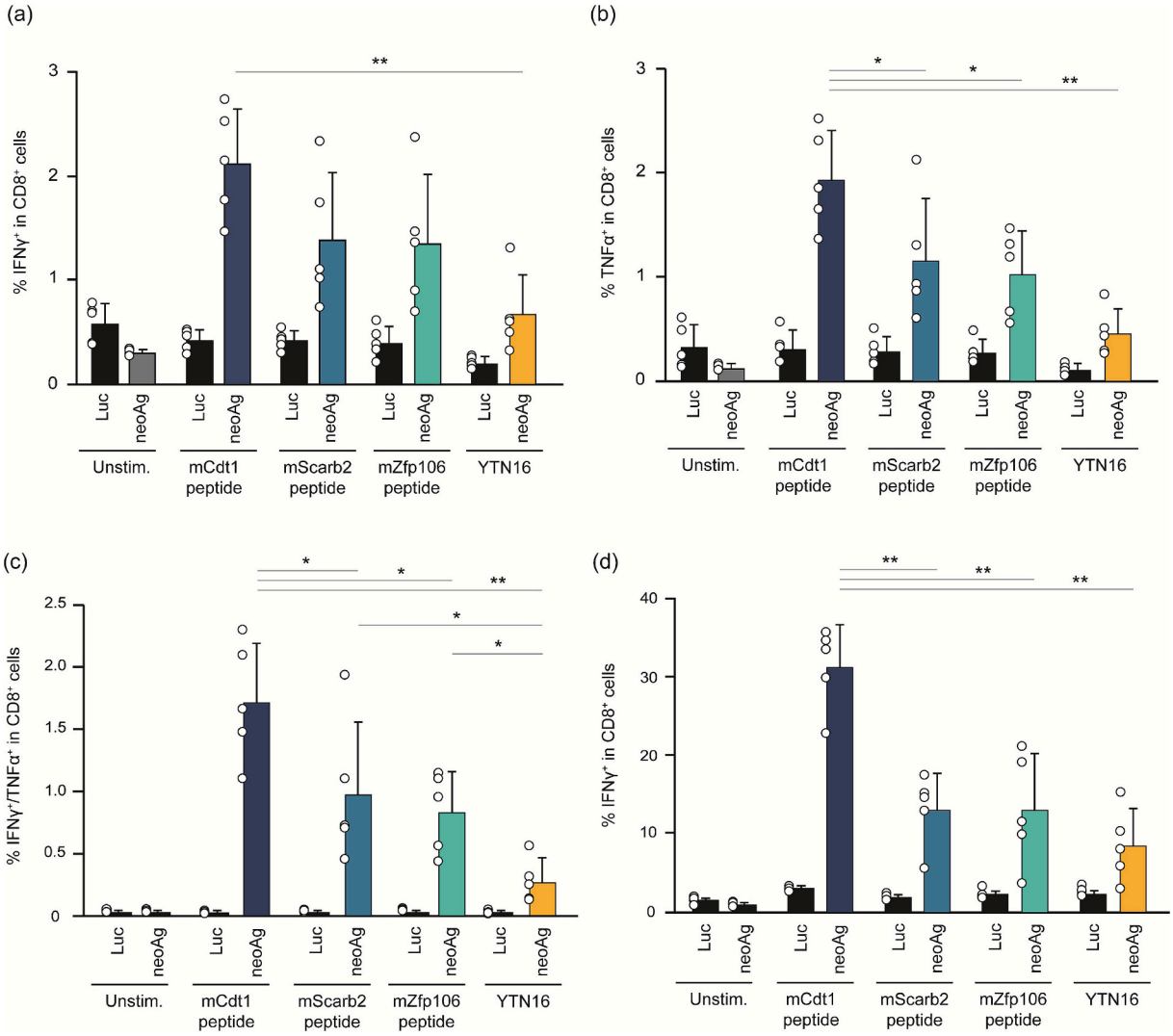

Fig. 6. Induction of tumor-reactive T cells by $LNP_{OP/EC}$.
Mice were treated as described in the legend for Fig. 5. Splenocytes from vaccinated mice were stimulated with the indicated neoantigen peptides or YTN16 tumor cells for 4 h, and cytokine production was assessed by intracellular cytokine staining. Bar graphs show the frequencies of (a) IFN-γ^+ cells, (b) TNF-α^+ cells, and (c) TNF-α^+IFN-γ^+ cells. For neoantigen-specific T cell expansion, splenocytes were cultured with RMA cells pulsed with mCdt1, mScarb2, and mZfp106 peptides for 6 days. On day 6, the expanded cells were stimulated with the indicated neoantigen peptides or YTN16 tumor cells for 4 h, and IFN-γ production was evaluated by intracellular cytokine staining. (d) The frequency of the IFN-γ^+ T cell population was expanded by in vitro stimulation. Scatter plots represent individual values; bar graphs represent the mean with SD ($n = 5$); $^{**}p < 0.01$, $^{*}p < 0.05$ (one-way ANOVA followed by SNK test). Original dot plots and gating strategies for flow cytometry analyses are provided in Supplementary Materials.

Furthermore, in vitro stimulation expanded the population of neoAg-specific $CD8^+$ T cells to approximately 30 % (Fig. 6d, Fig. S18). These results demonstrate that mRNA(neoAg)–$LNP_{OP/EC(20\%)}$ effectively induced $CD8^+$ T cells specific to all three encoded neoantigens.

3.6. $LNP_{OP/EC(20\%)}$ promotes antitumor responses by inducing neoAg-specific $CD8^+$ T cells

The capability of $LNP_{OP/EC(20\%)}$ to induce a neoAg-specific antitumor response was evaluated using the YTN16 tumor model. mRNA(neoAg)–$LNP_{OP/EC(20\%)}$ at a dose equivalent to 5.0 μg of mRNA was administered to YTN16-bearing mice twice, on days 7 and 14 post–tumor inoculation. $LNP_{OP/EC(20\%)}$ vaccination significantly suppressed YTN16 tumor growth compared with control groups, with strong inhibition observed following the booster immunization (Fig. 7a-c). In addition, immunized mice showed significantly reduced tumor volumes and tumor weights (Fig. 7d, e).

To further investigate the immune mechanisms underlying the antitumor effect, tumors were harvested and analyzed by flow cytometric analysis. The populations of both $CD45^+$ leukocytes and $CD8^+$ T cells were significantly higher in the $LNP_{OP/EC(20\%)}$–immunized group than in control groups (Fig. 7f, g). NeoAg-specific $CD8^+$ T cells were also significantly increased in vaccinated mice (Fig. 7h, Fig. S19b), including mCdt1–H-$2K^b$–dimer$^+$ T cells (Fig. 7i, Fig. S20a), mScarb2–H-$2D^b$–dimer$^+$ T cells (Fig. 7j, Fig. S20b), and mZfp106–H-$2D^b$–dimer$^+$ T cells (Fig. 7k, Fig. S20c). Collectively, mRNA(neoAg)–$LNP_{OP/EC(20\%)}$ vaccination effectively induced antigen-specific $CD8^+$ T cell populations corresponding to all three encoded neoantigens (mCdt1, mScarb2, and mZfp106), thereby contributing to the observed tumor regression in the YTN16 model.

4. Discussion

Lipid nanoparticles (LNPs) are known to exhibit intrinsic adjuvant properties, and several studies have demonstrated that even empty LNPs can enhance immune responses. For example, Acuitas Therapeutics'

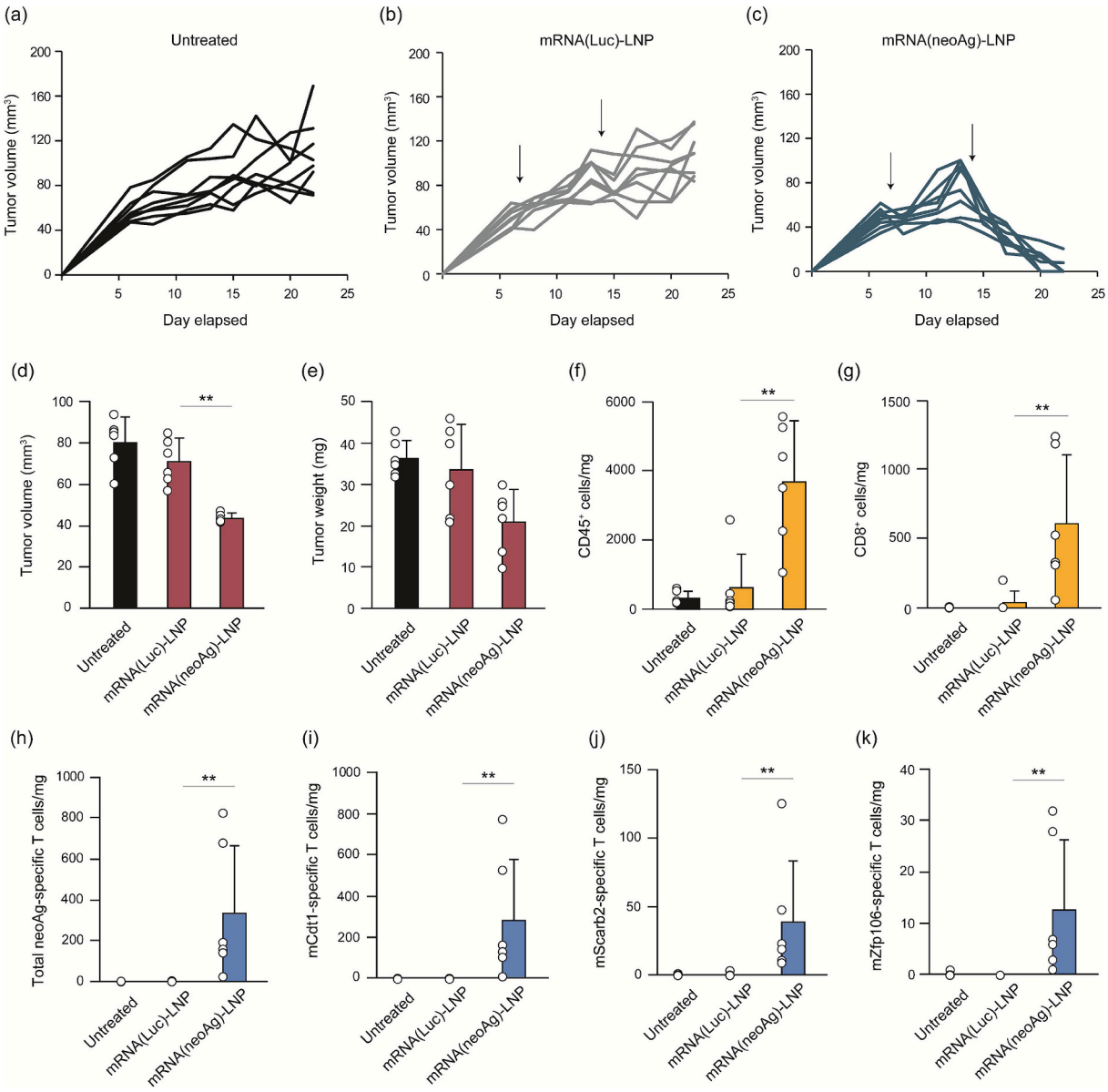

Fig. 7. Neoantigen-specific antitumor efficacy of mRNA(neoAg)–$LNP_{OP/EC(20\%)}$ in the YTN16 tumor model.
The therapeutic antitumor efficacy of $LNP_{OP/EC(20\%)}$ was evaluated in C57BL/6 J mice bearing YTN16 tumors. YTN16 cells (5.0×10^5 cells/200 μL) were inoculated into the abdominal flank ($n = 6$). Mice received two subcutaneous administrations of mRNA(neoAg)–$LNP_{OP/EC(20\%)}$ at a dose equivalent to 5.0 μg of mRNA on days 7 and 14 post-tumor inoculation. Tumor volumes were measured every 2 days for 3 weeks, with the endpoint defined as a tumor size of 1000 mm^3. Tumor volumes in (a) untreated, (b) mRNA(Luc)–$LNP_{OP/EC(20\%)}$, and (c) mRNA(neoAg)–$LNP_{OP/EC(20\%)}$ groups were measured until day 14 post-tumor inoculation. (d) Average tumor volumes and (e) tumor weights were calculated and statistically compared among groups. Flow cytometric analysis of tumor-derived immune cells: (f) $CD45^+$ cells, (g) $CD8^+$ T cells, (h) total neoAg-specific $CD8^+$ T cells, (i) mCdt1–H-$2K^b$–dimer$^+$, (j) mScarb2–H-$2D^b$–dimer$^+$, and (k) mZfp106–H-$2D^b$–dimer$^+$ populations. Scatter plots represent individual values; bar graphs represent the mean with SD ($n = 6$); $^{**}p < 0.01$, $^{*}p < 0.05$ (Mann–Whitney U test). Original dot plots and gating strategies for flow cytometry analyses are provided in Supplementary Materials.

proprietary LNPs have been shown to induce the maturation of monocyte-derived dendritic cells (MDDCs) by modulating the expression of CD40 and CD83 in human MDDCs, even in the absence of encapsulated mRNA [50]. These empty LNPs also stimulate the activation of T follicular helper (Tfh) cells and germinal centers (GC), both of which play essential roles in B cell responses to antigens [50,51]. When co-administered with recombinant antigen proteins, empty LNPs promote the maturation and differentiation of germinal center B cells [51], resulting in the production of antigen-specific antibodies at levels comparable to those induced by alum-based adjuvants [52]. Additionally, the topical application of empty LNPs has been found to induce pro-inflammatory chemokine production and monocyte infiltration at the injection site [53], both of which are key processes in recruiting immune cells and initiating a robust immune response. These observations emphasize the dual function of LNPs in mRNA vaccines, serving not only as delivery systems but also as potent adjuvants that enhance immunogenicity. The ionizable lipids within LNPs are believed to be primarily responsible for these adjuvant effects, as studies have shown that removing ionizable lipids from LNPs nearly abolishes their ability to stimulate immune response [51].

In this study, we focused on the application of vitamin E as a vaccine adjuvant, which is known to activate the immune system and serves as a key component of AS03, a squalene-based oil-in-water emulsion adjuvant used in avian influenza virus vaccines [54,55]. Studies have reported that vitamin E in the AS03-adjuvanted vaccines regulates the production of cytokines and chemokines such as CCL2, CCL3, IL-6, CSF3,

and CXCL1, while also facilitating monocyte antigen-loading and granulocyte recruitment [56]. The combination of vitamin E scaffolds and piperidine ring leads to the formation of ssPalmE. LNPs containing ssPalmE function not only as nucleic acid carriers but also as immune adjuvants, promoting the proliferation and differentiation of antigen-specific CD8+ T cells into effector and memory subsets and thereby stimulating cellular immunity [34]. It has been demonstrated that this activation of the cellular immune response is mediated through type I interferon signaling (IFN-β) [34]. Considering that dsDNA was detected at the skin (injection site) following the administration of $LNP_{ssPalmE}$, the vitamin E scaffolds are thought to induce damage-associated molecular patterns (DAMPs)–mediated activation of pattern recognition receptors (PRR) signaling, thereby triggering the type I interferon pathway [34]. Previous studies have shown that inhibition of type I interferon signaling in mRNA(OVA)–$LNP_{ssPalmE}$–immunized OT-I mice significantly reduced splenic OVA-specific $CD8^+$ T cell numbers, downregulated CD62L expression on $CD8^+$ T cells, and suppressed IL-2 and IFN-γ production by $CD8^+$ T cells [34]. In the current study, we aimed to evaluate the role of type I interferon signaling in the capability of $LNP_{OP/EC(20\%)}$ to induce immune responses. Accordingly, wild-type mice were pretreated with a blocking antibody against the interferon-α/β receptor α chain (anti-IFNAR-1 mAb) before LNP immunization. CTL assays demonstrated that anti-IFNAR-1 pretreatment tended to reduce the CTL activity in mice administered with either mRNA(OVA)–$LNP_{OP/EC(20\%)}$ (Fig. S21a) or empty-$LNP_{OP/EC(20\%)}$ co-administered with recombinant OVA (Fig. S21b). These results are consistent with previous findings and support the conclusion that activation of type I interferon signaling is critical for the ability of LNPs containing vitamin E scaffolds to induce robust cellular immune responses. However, since the CTL activity was not completely abolished, other pathways of immune activation might also contribute to the vaccine efficacy of $LNP_{OP/EC(20\%)}$.

The ssPalmO-Phe is another derivative of ssPalm that has been explored for its applications in gene therapy, in contrast to ssPalmE, which is primarily used in vaccine formulations. $LNP_{ssPalmO\text{-}Phe}$ has been demonstrated to possess high gene transfer efficiency and reduced immune-stimulatory properties, making it a promising candidate material for gene therapy [36,40,57]. The ssPalmO-Phe incorporates a phenyl ester group and oleic acid (phenyl oleate) as the hydrophobic scaffolds. In general, ester and/or disulfide bonds are integrated into ionizable lipids to promote biodegradation, a strategy designed to minimize adverse side effects resulting from the accumulation of lipid-like substances [35]. The combination of disulfide bonds and phenyl ester groups has been observed to significantly enhance the mRNA transfection activity by facilitating a self-degradation process within the compact particle structure, which subsequently promotes the release of the nucleic acid cargo [35,36].

In our preliminary experiments, we found that ssPalmE exhibited an approximately 30-fold lower gene expression compared with ssPalmO-Phe (Fig. S1b). Although its gene expression is inherently low, ssPalmE demonstrates distinct and highly relevant adjuvant activity for cancer vaccines [34,41]. A simple strategy to add vitamin E and its derivative (α-tocopherol and α-tocopherol succinate) to $LNP_{ssPalmO\text{-}Phe}$, enhanced CTL activity in a vitamin *E*-dependent manner (Fig. S22). This finding indicates that the balance between vitamin E (immunogenic properties) and phenyl oleate (gene transfection efficiency) determines the overall vaccine efficacy of the combined LNP formulation. In our previous study, a self-degradable moiety was chemically combined with a vitamin E scaffold to develop an ionizable lipid more suitable for vaccine application, resulting in the formation of ssPalmE-Phe. This ionizable lipid demonstrated both enhanced gene expression and adjuvant activity [42]. However, because the self-degradable moiety and vitamin E were directly linked in a fixed one-to-one ratio, further optimization of the balance between self-degradability and adjuvanticity was limited. From a practical standpoint, ssPalmE-Phe, which contains two phenyl ester groups and two tocopherols, also presented handling challenges due to its extreme hydrophobicity. To address these limitations, we adopted a simplified strategy by combining the ionizable lipids ssPalmE (vitamin E) and ssPalmO-Phe (phenyl oleate) separately to create $LNP_{OP/EC}$, allowing us to modify its composition and formulation to evaluate its efficacy as an mRNA vaccine carrier.

Immune response assessments showed that increasing ssPalmE content in $LNP_{OP/EC}$ correlated with enhanced CTL activity (Fig. 1c) and IL-6 production (Fig. 2a-d), reinforcing the immunogenic role of vitamin E. However, no significant differences were observed in antigen-specific total IgG levels across all groups (Fig. S4). Conversely, evaluation of in vivo gene expression revealed that higher ssPalmE content reduced the gene transfection efficiency of $LNP_{OP/EC}$ (Fig. 1d, e). These results suggest that LNP formulations inherently possess strong adjuvant activity, contributing particularly to humoral immunity, whereas excessive incorporation of ssPalmE compromises gene delivery. Therefore, the overall lipid composition must be optimized to balance the immune stimulation and transfection efficiency.

In a previous study, $LNP_{ssPalmE}$ was formulated with 60 % of ionizable lipid ssPalmE solely to exploit its immune-adjuvant effect [34]. However, in our subsequent work, we demonstrated that a cholesterol content of 40 % is also critical for immune-adjuvant activity [42,58]. Our findings further showed that the structural properties of LNPs contribute to immune stimulation. While ionizable lipids play a key role in immune activation, the degree of immune responses is more strongly influenced by the cholesterol content. In particular, cholesterol levels between 40 and 60 % promote a nano-sized, intermediate bilayer-like structure that directly affects both LNP morphology and immune-stimulating function [58]. Since increasing the ssPalmE content induced inflammatory responses (Fig. 1c), in this study, we fixed cholesterol content at 40 % and focused on identifying the optimal ssPalmE content for $LNP_{OP/EC}$. Evaluation of lipid composition revealed that 40 % cholesterol and 7.5 % DOPC were essential for the transfection activity of $LNP_{OP/EC(20\%)}$ (Fig. S6a–c). These results are consistent with previous findings showing that, although the proportion of ionizable lipid is the primary determinant of LNP activity, a delicate balance among ionizable lipids, phospholipids, and cholesterol is crucial for optimizing both gene transfection efficiency and immune activation by LNPs. Notably, the $LNP_{OP/EC}$ (ssPalmE content: 5–30 %) contained the same amount of cholesterol, suggesting that all the LNPs possessed a baseline level of adjuvant activity. Further increases in adjuvant properties and reductions in gene expression caused by the addition of ssPalmE do not necessarily improve the antibody production.

Studies indicate that the upregulation of cytokine IL-6 in response to LNP formulations used in mRNA therapies can reflect their immunogenicity and potential toxicity [59]. This highlights the importance of optimizing LNP formulations to minimize adverse effects while maintaining the vaccine efficacy. Considering the vaccine efficacy, gene transfection efficiency, and the safety of formulation, $LNP_{OP/EC}$ with 20–25 % of ssPalmE content appeared to be optimal. The cytokine IL-6 response induced by $LNP_{OP/EC(20\%)}$ was transient, peaking at 6 h post-injection and declining to the baseline by 24 h (Fig. 2a-d), indicating a short-lived inflammatory response with minimal risk of adverse effects.

The vaccination efficacy of $LNP_{OP/EC(20\%)}$ was also influenced by the overall LNP concentration. As shown in Fig. 3, the CTL activity of $LNP_{OP/EC(20\%)}$ decreased when the L/R ratio was too low (33 nmol/μg) or too high (200 nmol/μg). The reduced CTL activity at an L/R of 33 nmol/μg suggests that both the LNP concentration and the vitamin E content are crucial for inducing cell-mediated immunity. Conversely, an excessively high concentration of $LNP_{OP/EC}$ reduced vaccination activity, likely due to toxicity associated with high LNP concentrations. A previous study reported that administering a high dose of mRNA–LNP significantly upregulated gene transcripts associated with monocyte/granulocyte recruitment and inflammasome activation (e.g., *Il1b* and *Nlrp3*), as well as pro-apoptotic and necroptotic pathways [53]. It was also reported that immune responses triggered by a booster dose of mRNA–LNP vaccination may exacerbate adverse side effects, potentially causing tissue damage and intensifying inflammatory reactions [53]. Therefore,

excessive immune activation by mRNA–$LNP_{OP/EC(20\%)}$ with an L/R ratio of 200 nmol/μg was not beneficial for vaccine efficacy and resulted in lower antigen-specific total IgG levels compared with other groups (Fig. 3a-c).

mRNA(OVA)-$LNP_{OP/EC(20\%)}$ demonstrated robust antitumor efficacy against the E.G7-OVA tumor model (Fig. 4), consistent with the results of cellular immunity evaluation (Fig. 1c and 3a). The antitumor response was closely associated with the induction of OVA-specific $CD8^+$ T cells. The expansion of antigen-specific $CD8^+$ TILs population within the tumor indicated a targeted immune activation rather than a broad, nonspecific response. These $CD8^+$ TILs were also functionally active, expressing Granzyme B (cytotoxic molecule) (Fig. 4f) and producing IFN-γ (Fig. 4g, h) upon antigen stimulation. These characteristics signify a functional Tc1/Th-1 type immune response, which plays a central role in effective tumor suppression [60,61]. Collectively, these findings suggest that $LNP_{OP/EC(20\%)}$ not only expands antigen-specific $CD8^+$ T cells but also provides them with strong effector functions that mediate antitumor activity. However, it should be noted that ovalbumin possesses strong intrinsic antigenicity in murine models, limiting its translational relevance to clinical applications.

Neoantigens, derived from somatic genomic mutations in mouse cells, generally exhibit lower antigenicity due to minimal variations in their amino acid sequences. To evaluate the applicability of $LNP_{OP/EC(20\%)}$ as a cancer vaccine carrier in a clinically relevant context, we investigated its immune-stimulatory activity in a YTN16 tumor model. YTN16, a murine gastric cancer cell line, has three neoepitopes: mCdt1, mScarb2, and mZfp106 [37,38]. A previous study reported that dendritic cells (DCs) pulsed with these neopeptides inhibited tumor growth in YTN16 tumor-bearing mice and induced mCdt1-, mScarb2-, and mZfp106-reactive $CD8^+$ T cells in the spleen [49]. Administration of mRNA(neoAg)–$LNP_{OP/EC(20\%)}$ in the YTN16 tumor model successfully activated neoAg-specific T cells. mRNA(neoAg)-$LNP_{OP/EC(20\%)}$ elicited strong IFN-γ (Fig. 6a) and TNF-α (Fig. 6b) production in response to mCdt1, mScarb2, and mZfp106 peptide stimulation, indicating robust neoAg-specific immune activation. $LNP_{OP/EC(20\%)}$ also suppressed tumor growth effectively, with further inhibition observed after the booster dose (Fig. 7c), suggesting that repeated vaccination enhances therapeutic efficacy. Notably, several distinct neoAg-specific mCdt1–H-$2K^{b+}$, mScarb2–H-$2D^{b+}$, and mZfp106–H-$2D^{b+}$ $CD8^+$ T-cell populations were detected (Fig. 7h-k), confirming that the tandem minigene vaccine encoding mCdt1, mScarb2, and mZfp106 effectively induced $CD8^+$ T cell responses specific to all three neoantigens. Such multi-targeted induction is particularly important in cancer immunotherapy, as it can reduce the likelihood of immune escape caused by the loss of individual tumor antigens [62,63]. Overall, these findings demonstrated that $LNP_{OP/EC(20\%)}$ exhibits potent immune-stimulatory activity and efficient antigen delivery, highlighting its potential as a versatile platform for cancer immunotherapy.

5. Conclusion

Vitamin E moiety enhanced the activation of cellular immunity. This strong immune activation not only promoted model antigen-specific responses but also elicited robust neoantigen-specific responses. The efficiency of gene delivery and immune activation by ionizable lipids varies greatly depending on their chemical structure, and achieving optimal therapeutic outcomes with a single type of ionizable lipid can be challenging in some situations. Furthermore, strategies that rely on chemically linking multiple functional moieties may face practical limitations in synthesis and handling. In contrast, combining ionizable lipids with distinct functionalities offers a flexible and effective approach to balance the transfection efficiency and immunostimulatory capacity. This strategy may provide valuable insights not only for the development of cancer vaccines but also for a wide range of mRNA–LNP–based therapeutic applications.

CRediT authorship contribution statement

Jessica Anindita: Writing – review & editing, Writing – original draft, Visualization, Validation, Methodology, Investigation, Formal analysis, Data curation, Conceptualization. **Hiroki Tanaka:** Writing – review & editing, Writing – original draft, Validation, Project administration, Funding acquisition, Conceptualization. **Ryotaro Oyama:** Investigation, Data curation. **Atsuya Matsumaru:** Investigation, Data curation. **Yuta Nakai:** Resources, Investigation, Conceptualization. **Kota Tange:** Resources, Investigation, Data curation. **Koji Nagaoka:** Writing – original draft, Project administration, Methodology, Investigation, Formal analysis, Data curation. **Hideyuki Nakanishi:** Writing – original draft, Resources, Project administration, Investigation. **Takeshi Kawamura:** Writing – review & editing, Resources. **Toshiya Tanaka:** Writing – review & editing, Resources. **Takefumi Yamashita:** Writing – review & editing, Resources. **Akihiro Kuroda:** Writing – review & editing, Resources. **Sachiyo Nomura:** Writing – review & editing, Resources. **Hiroto Hatakeyama:** Writing – review & editing, Supervision. **Keiji Itaka:** Writing – review & editing, Supervision. **Tatsuhiko Kodama:** Writing – review & editing, Supervision. **Kazuhiro Kakimi:** Writing – review & editing, Supervision. **Hidetaka Akita:** Writing – review & editing, Writing – original draft, Supervision, Project administration, Funding acquisition, Conceptualization.

Funding

H. Tanaka was supported by the JSPS KAKENHI [18K18377, 21K18035]. H. Akita was supported by a JST CREST grant [grant number JPMJCR17H1], JSPS KAKENHI [grant numbers 20H00657, 21K18320], Basic Science and Platform Technology Program for Innovative Biological Medicine from the Japan Agency for Medical Research and Development (AMED) under Grant Number JP21gm1610006, and the Canon Foundation Research Grant Program. K. Itaka was supported by the Japan Agency for Medical Research and Development (AMED) under Grant Number JP223fa627002 (K.I.). H. Tanaka and H. Akita were funded by NOF CORPORATION as joint research. This work was partially supported by JSPS KAKENHI Grant Number JP24K02393.

Declaration of competing interest

This research was partially conducted as joint research between Tohoku University, Chiba University, and NOF CORPORATION. The remaining funding organizations had no roles in the design, collection, analyses, or interpretation of data for this study. These organizations also had no roles in either the writing of the manuscript or in the decision to publish the results.

H.T., Y.N., K.T., and H.A. hold a relative patent pending number WO/2019/188867. H.T., Y.N., K.T., and H.A. hold a relative patent pending number WO/2021/060440. H.T., Y.N., K.T., and H.A., hold a relative patent pending number WO/2023/190170. H.T., J.A., R.O., Y. N., K.T., and H.A., hold a relative patent pending number WO/2024/014511. Y.N. and K.T. are employed by NOF CORPORATION. H.T. and H.A. have received consultant fees from NOF CORPORATION.

Acknowledgement

The authors wish to thank James L. McDonald for his helpful advice in writing the English manuscript.

Appendix A. Supplementary data

Supplementary data to this article can be found online at https://doi.org/10.1016/j.jconrel.2025.114414.

Data availability

Data will be made available on request.

References

[1] C. Zhang, G. Maruggi, H. Shan, J. Li, Advances in mRNA vaccines for infectious diseases, Front. Immunol. 10 (2019) 594.
[2] N. Pardi, M.J. Hogan, F.W. Porter, D. Weissman, mRNA vaccines — a new era in vaccinology, Nat. Rev. Drug Discov. 17 (4) (2018) 261–279.
[3] X.-J. Han, X.-L. Ma, L. Yang, Y.-Q. Wei, Y. Peng, X.-W. Wei, Progress in neoantigen targeted cancer immunotherapies, Front. Cell Dev. Biol. 8 (2020), https://doi.org/10.3389/fcell.2020.00728.
[4] P.D. Katsikis, K.J. Ishii, C. Schliehe, Challenges in developing personalized neoantigen cancer vaccines, Nat. Rev. Immunol. 24 (2024) 213–227.
[5] N. Xie, G. Shen, W. Gao, Z. Huang, C. Huang, L. Fu, Neoantigens: promising targets for cancer therapy, Signal Transduct. Target. Ther. 8 (2023) 1–38.
[6] U. Sahin, E. Derhovanessian, M. Miller, B.-P. Kloke, P. Simon, M. Löwer, V. Bukur, A.D. Tadmor, U. Luxemburger, B. Schrörs, T. Omokoko, M. Vormehr, C. Albrecht, A. Paruzynski, A.N. Kuhn, J. Buck, S. Heesch, K.H. Schreeb, F. Müller, I. Ortseifer, I. Vogler, E. Godehardt, S. Attig, R. Rae, A. Breitkreuz, C. Tolliver, M. Suchan, G. Martic, A. Hohberger, P. Sorn, J. Diekmann, J. Ciesla, O. Waksmann, A.-K. Brück, M. Witt, M. Zillgen, A. Rothermel, B. Kasemann, D. Langer, S. Bolte, M. Diken, S. Kreiter, R. Nemecek, C. Gebhardt, S. Grabbe, C. Höller, J. Utikal, C. Huber, C. Loquai, Ö. Türeci, Personalized RNA mutanome vaccines mobilize poly-specific therapeutic immunity against cancer, Nature 547 (2017) 222–226.
[7] G. Cafri, J.J. Gartner, T. Zaks, K. Hopson, N. Levin, B.C. Paria, M.R. Parkhurst, R. Yossef, F.J. Lowery, M.S. Jafferji, T.D. Prickett, S.L. Goff, C.T. McGowan, S. Seitter, M.L. Shindorf, A. Parikh, P.D. Chatani, P.F. Robbins, S.A. Rosenberg, mRNA vaccine–induced neoantigen-specific T cell immunity in patients with gastrointestinal cancer, J. Clin. Invest. 130 (2020) 5976–5988.
[8] M. Schmidt, I. Vogler, E. Derhovanessian, T. Omokoko, E. Godehardt, S. Attig, A. Cortini, S. Newrzela, J. Grützner, S. Bolte, D. Langer, M. Eichbaum, H. Lindman, S. Pascolo, A. Schneeweiss, T. Sjöblom, Ö. Türeci, U. Sahin, 88MO T-cell responses induced by an individualized neoantigen specific immune therapy in post (neo) adjuvant patients with triple negative breast cancer, Ann. Oncol. 31 (2020) S276.
[9] Z. Deng, Y. Tian, J. Song, G. An, P. Yang, mRNA vaccines: the dawn of a new era of cancer immunotherapy, Front. Immunol. 13 (2022), https://doi.org/10.3389/fimmu.2022.887125.
[10] J.S. Weber, M.S. Carlino, A. Khattak, T. Meniawy, G. Ansstas, M.H. Taylor, K. B. Kim, M. McKean, G.V. Long, R.J. Sullivan, M. Faries, T.T. Tran, C.L. Cowey, A. Pecora, M. Shaheen, J. Segar, T. Medina, V. Atkinson, G.T. Gibney, J.J. Luke, S. Thomas, E.I. Buchbinder, J.A. Healy, M. Huang, M. Morrissey, I. Feldman, V. Sehgal, C. Robert-Tissot, P. Hou, L. Zhu, M. Brown, P. Aanur, R.S. Meehan, T. Zaks, Individualised neoantigen therapy mRNA-4157 (V940) plus pembrolizumab versus pembrolizumab monotherapy in resected melanoma (KEYNOTE-942): a randomised, phase 2b study, Lancet 403 (2024) 632–644.
[11] F. Braiteh, P. LoRusso, A. Balmanoukian, S. Klempner, D.R. Camidge, M. Hellmann, M. Gordon, J. Bendell, L. Mueller, R. Sabado, P. Twomey, L. Delamarre, J. Huang, M. Yadav, J. Zhang, P. McDonald, F. Müller, E. Derhovanessian, Ö. Türeci, U. Sahin, L. Siu, Abstract CT169: a phase Ia study to evaluate RO7198457, an individualized Neoantigen Specific immunoTherapy (iNeST), in patients with locally advanced or metastatic solid tumors, Cancer Res. 80 (2020) CT169.
[12] L.A. Rojas, Z. Sethna, K.C. Soares, C. Olcese, N. Pang, E. Patterson, J. Lihm, N. Ceglia, P. Guasp, A. Chu, R. Yu, A.K. Chandra, T. Waters, J. Ruan, M. Amisaki, A. Zebboudj, Z. Odgerel, G. Payne, E. Derhovanessian, F. Müller, I. Rhee, M. Yadav, A. Dobrin, M. Sadelain, M. Łuksza, N. Cohen, L. Tang, O. Basturk, M. Gönen, S. Katz, R.K. Do, A.S. Epstein, P. Momtaz, W. Park, R. Sugarman, A.M. Varghese, E. Won, A. Desai, A.C. Wei, M.I. D'Angelica, T.P. Kingham, I. Mellman, T. Merghoub, J.D. Wolchok, U. Sahin, Ö. Türeci, B.D. Greenbaum, W.R. Jarnagin, J. Drebin, E.M. O'Reilly, V.P. Balachandran, Personalized RNA neoantigen vaccines stimulate T cells in pancreatic cancer, Nature 618 (2023) 144–150.
[13] E. Decroly, F. Ferron, J. Lescar, B. Canard, Conventional and unconventional mechanisms for capping viral mRNA, Nat. Rev. Microbiol. 10 (2011) 51–65.
[14] A. Ramanathan, G.B. Robb, S.-H. Chan, mRNA capping: biological functions and applications, Nucleic Acids Res. 44 (2016) 7511–7526.
[15] L.A. Passmore, J. Coller, Roles of mRNA poly(A) tails in regulation of eukaryotic gene expression, Nat. Rev. Mol. Cell Biol. 23 (2022) 93–106.
[16] C.R. Eckmann, C. Rammelt, E. Wahle, Control of poly(A) tail length, Wiley Interdiscip. Rev. RNA 2 (2011) 348–361.
[17] K. Karikó, H. Muramatsu, F.A. Welsh, J. Ludwig, H. Kato, S. Akira, D. Weissman, Incorporation of Pseudouridine into mRNA yields superior nonimmunogenic vector with increased translational capacity and biological stability, Mol. Ther. 16 (2008) 1833–1840.
[18] O. Andries, S. Mc Cafferty, S.C. De Smedt, R. Weiss, N.N. Sanders, T. Kitada, N1-methylpseudouridine-incorporated mRNA outperforms pseudouridine-incorporated mRNA by providing enhanced protein expression and reduced immunogenicity in mammalian cell lines and mice, J. Control. Release 217 (2015) 337–344.
[19] M. Baiersdörfer, G. Boros, H. Muramatsu, A. Mahiny, I. Vlatkovic, U. Sahin, K. Karikó, A facile method for the removal of dsRNA contaminant from in vitro-transcribed mRNA, Mol. Ther. Nucleic Acids 15 (2019) 26–35.
[20] X. Piao, V. Yadav, E. Wang, W. Chang, L. Tau, B.E. Lindenmuth, S.X. Wang, Double-stranded RNA reduction by chaotropic agents during in vitro transcription of messenger RNA, Mol. Ther. Nucleic Acids 29 (2022) 618–624.
[21] P. Huang, H. Deng, Y. Zhou, X. Chen, The roles of polymers in mRNA delivery, Matter 5 (2022) 1670–1699.
[22] W. Yang, L. Mixich, E. Boonstra, H. Cabral, Polymer-based mRNA delivery strategies for advanced therapies, Adv. Healthc. Mater. 12 (2023), https://doi.org/10.1002/adhm.202202688.
[23] X. Hou, T. Zaks, R. Langer, Y. Dong, Lipid nanoparticles for mRNA delivery, Nat. Rev. Mater. 6 (12) (2021) 1078–1094.
[24] R. Tenchov, R. Bird, A.E. Curtze, Q. Zhou, Lipid nanoparticles—from liposomes to mRNA vaccine delivery, a landscape of research diversity and advancement, ACS Nano 15 (2021) 16982–17015.
[25] L.A. Jackson, E.J. Anderson, N.G. Rouphael, P.C. Roberts, M. Makhene, R.N. Coler, M.P. McCullough, J.D. Chappell, M.R. Denison, L.J. Stevens, A.J. Pruijssers, A. McDermott, B. Flach, N.A. Doria-Rose, K.S. Corbett, K.M. Morabito, S. O'Dell, S. D. Schmidt, P.A. Swanson, M. Padilla, J.R. Mascola, K.M. Neuzil, H. Bennett, W. Sun, E. Peters, M. Makowski, J. Albert, K. Cross, W. Buchanan, R. Pikaart-Tautges, J.E. Ledgerwood, B.S. Graham, J.H. Beigel, An mRNA vaccine against SARS-CoV-2 — preliminary report, N. Engl. J. Med. 383 (2020) 1920–1931.
[26] L.R. Baden, H.M. El Sahly, B. Essink, K. Kotloff, S. Frey, R. Novak, D. Diemert, S. A. Spector, N. Rouphael, C.B. Creech, J. McGettigan, S. Khetan, N. Segall, J. Solis, A. Brosz, C. Fierro, H. Schwartz, K. Neuzil, L. Corey, P. Gilbert, H. Janes, D. Follmann, M. Marovich, J. Mascola, L. Polakowski, J. Ledgerwood, B.S. Graham, H. Bennett, R. Pajon, C. Knightly, B. Leav, W. Deng, H. Zhou, S. Han, M. Ivarsson, J. Miller, T. Zaks, Efficacy and safety of the mRNA-1273 SARS-CoV-2 vaccine, N. Engl. J. Med. 384 (2021) 403–416.
[27] E.E. Walsh, R.W. Frenck, A.R. Falsey, N. Kitchin, J. Absalon, A. Gurtman, S. Lockhart, K. Neuzil, M.J. Mulligan, R. Bailey, K.A. Swanson, P. Li, K. Koury, W. Kalina, D. Cooper, C. Fontes-Garfias, P.-Y. Shi, Ö. Türeci, K.R. Tompkins, K. E. Lyke, V. Raabe, P.R. Dormitzer, K.U. Jansen, U. Şahin, W.C. Gruber, Safety and immunogenicity of two RNA-based Covid-19 vaccine candidates, N. Engl. J. Med. 383 (2020) 2439–2450.
[28] F.P. Polack, S.J. Thomas, N. Kitchin, J. Absalon, A. Gurtman, S. Lockhart, J. L. Perez, G. Pérez Marc, E.D. Moreira, C. Zerbini, R. Bailey, K.A. Swanson, S. Roychoudhury, K. Koury, P. Li, W.V. Kalina, D. Cooper, R.W. Frenck, L. L. Hammitt, Ö. Türeci, H. Nell, A. Schaefer, S. Ünal, D.B. Tresnan, S. Mather, P. R. Dormitzer, U. Şahin, K.U. Jansen, W.C. Gruber, Safety and efficacy of the BNT162b2 mRNA Covid-19 vaccine, N. Engl. J. Med. 383 (2020) 2603–2615.
[29] S.H. Kiaie, N. Majidi Zolbanin, A. Ahmadi, R. Bagherifar, H. Valizadeh, F. Kashanchi, R. Jafari, Recent advances in mRNA-LNP therapeutics: immunological and pharmacological aspects, J. Nanobiotechnol. 20 (2022) 276.
[30] B.Z. Igyártó, Z. Qin, The mRNA-LNP vaccines – the good, the bad and the ugly? Front. Immunol. 15 (2024) https://doi.org/10.3389/fimmu.2024.1336906.
[31] C. Hald Albertsen, J.A. Kulkarni, D. Witzigmann, M. Lind, K. Petersson, J. B. Simonsen, The role of lipid components in lipid nanoparticles for vaccines and gene therapy, Adv. Drug Deliv. Rev. 188 (2022) 114416.
[32] X. Han, H. Zhang, K. Butowska, K.L. Swingle, M.-G. Alameh, D. Weissman, M. J. Mitchell, An ionizable lipid toolbox for RNA delivery, Nat. Commun. 12 (2021) 7233.
[33] J. Li, J. Hu, D. Jin, H. Huo, N. Chen, J. Lin, X. Lu, High-throughput synthesis and optimization of ionizable lipids through A3 coupling for efficient mRNA delivery, J. Nanobiotechnol. 22 (2024) 672.
[34] R. Oyama, H. Ishigame, H. Tanaka, N. Tateshita, M. Itazawa, R. Imai, N. Nishiumi, J.-I. Kishikawa, T. Kato, J. Anindita, Y. Nishikawa, M. Maeki, M. Tokeshi, K. Tange, Y. Nakai, Y. Sakurai, T. Okada, H. Akita, An ionizable lipid material with a vitamin E scaffold as an mRNA vaccine platform for efficient cytotoxic T cell responses, ACS Nano 17 (2023) 18758–18774.
[35] H. Tanaka, Y. Sakurai, J. Anindita, H. Akita, Development of lipid-like materials for RNA delivery based on intracellular environment-responsive membrane destabilization and spontaneous collapse, Adv. Drug Deliv. Rev. 154–155 (2020) 210–226.
[36] H. Tanaka, T. Takahashi, M. Konishi, N. Takata, M. Gomi, D. Shirane, R. Miyama, S. Hagiwara, Y. Yamasaki, Y. Sakurai, K. Ueda, K. Higashi, K. Moribe, E. Shinsho, R. Nishida, K. Fukuzawa, E. Yonemochi, K. Okuwaki, Y. Mochizuki, Y. Nakai, K. Tange, H. Yoshioka, S. Tamagawa, H. Akita, Self-degradable lipid-like materials based on "hydrolysis accelerated by the intra-particle enrichment of reactant (HyPER)" for messenger RNA delivery, Adv. Funct. Mater. 30 (2020) 1910575.
[37] M. Yamamoto, S. Nomura, A. Hosoi, K. Nagaoka, T. Iino, T. Yasuda, T. Saito, H. Matsushita, E. Uchida, Y. Seto, J.R. Goldenring, K. Kakimi, M. Tatematsu, T. Tsukamoto, Established gastric cancer cell lines transplantable into C57 BL /6 mice show fibroblast growth factor receptor 4 promotion of tumor growth, Cancer Sci. 109 (2018) 1480–1492.
[38] K. Nagaoka, H. Nakanishi, H. Tanaka, J. Anindita, T. Kawamura, T. Tanaka, T. Yamashita, A. Kuroda, S. Nomura, H. Akita, K. Itaka, T. Kodama, K. Kakimi, Neoantigen mRNA vaccines induce progenitor-exhausted T cells that support anti-PD-1 therapy in gastric cancer with peritoneal metastasis, Gastric Cancer 28 (2025) 825–836.
[39] H. Akita, Y. Noguchi, H. Hatakeyama, Y. Sato, K. Tange, Y. Nakai, H. Harashima, Molecular tuning of a vitamin E-scaffold pH-sensitive and reductive cleavable lipid-like material for accelerated in vivo hepatic siRNA delivery, ACS Biomater Sci. Eng. 1 (2015) 834–844.
[40] H. Tanaka, S. Hagiwara, D. Shirane, T. Yamakawa, Y. Sato, C. Matsumoto, K. Ishizaki, M. Hishinuma, K. Chida, K. Sasaki, E. Yonemochi, K. Ueda, K. Higashi, K. Moribe, T. Tadokoro, K. Maenaka, S. Taneichi, Y. Nakai, K. Tange, Y. Sakurai,

H. Akita, Ready-to-use-type lyophilized lipid nanoparticle formulation for the Postencapsulation of messenger RNA, ACS Nano 17 (2023) 2588–2601.
[41] N. Tateshita, N. Miura, H. Tanaka, T. Masuda, S. Ohtsuki, K. Tange, Y. Nakai, H. Yoshioka, H. Akita, Development of a lipoplex-type mRNA carrier composed of an ionizable lipid with a vitamin E scaffold and the KALA peptide for use as an ex vivo dendritic cell-based cancer vaccine, J. Control. Release 310 (2019) 36–46.
[42] J. Anindita, H. Tanaka, R. Oyama, S. Hagiwara, D. Shirane, S. Taneichi, Y. Nakai, K. Tange, H. Hatakeyama, Y. Sakurai, H. Akita, Development of a ready-to-use-type RNA vaccine carrier based on an intracellular environment-responsive lipid-like material with immune-activating vitamin E scaffolds, Pharmaceutics 15 (2023) 2702.
[43] K.J. Hassett, K.E. Benenato, E. Jacquinet, A. Lee, A. Woods, O. Yuzhakov, S. Himansu, J. Deterling, B.M. Geilich, T. Ketova, C. Mihai, A. Lynn, I. McFadyen, M.J. Moore, J.J. Senn, M.G. Stanton, Ö. Almarsson, G. Ciaramella, L.A. Brito, Optimization of lipid nanoparticles for intramuscular administration of mRNA vaccines, Mol. Ther. Nucleic Acids 15 (2019) 1–11.
[44] K.S. Corbett, D.K. Edwards, S.R. Leist, O.M. Abiona, S. Boyoglu-Barnum, R. A. Gillespie, S. Himansu, A. Schäfer, C.T. Ziwawo, A.T. DiPiazza, K.H. Dinnon, S. M. Elbashir, C.A. Shaw, A. Woods, E.J. Fritch, D.R. Martinez, K.W. Bock, M. Minai, B.M. Nagata, G.B. Hutchinson, K. Wu, C. Henry, K. Bahl, D. Garcia-Dominguez, L. Z. Ma, I. Renzi, W.P. Kong, S.D. Schmidt, L. Wang, Y. Zhang, E. Phung, L.A. Chang, R.J. Loomis, N.E. Altaras, E. Narayanan, M. Metkar, V. Presnyak, C. Liu, M. K. Louder, W. Shi, K. Leung, E.S. Yang, A. West, K.L. Gully, L.J. Stevens, N. Wang, D. Wrapp, N.A. Doria-Rose, G. Stewart-Jones, H. Bennett, G.S. Alvarado, M. C. Nason, T.J. Ruckwardt, J.S. McLellan, M.R. Denison, J.D. Chappell, I.N. Moore, K.M. Morabito, J.R. Mascola, R.S. Baric, A. Carfi, B.S. Graham, SARS-CoV-2 mRNA vaccine design enabled by prototype pathogen preparedness, Nature 586 (7830) (2020) 567–571.
[45] X. Du, E. Yada, Y. Terai, T. Takahashi, H. Nakanishi, H. Tanaka, H. Akita, K. Itaka, Comprehensive evaluation of lipid nanoparticles and polyplex nanomicelles for muscle-targeted mRNA delivery, Pharmaceutics 15 (2023) 2291.
[46] Y. Lee, M. Jeong, J. Park, H. Jung, H. Lee, Immunogenicity of lipid nanoparticles and its impact on the efficacy of mRNA vaccines and therapeutics, Exp. Mol. Med. 55 (2023) 2085–2096.
[47] Z.L.Z. Hay, J.E. Slansky, Granzymes: the molecular executors of immune-mediated cytotoxicity, Int. J. Mol. Sci. 23 (2022) 1833.
[48] M.J. Pinkoski, N.J. Waterhouse, J.A. Heibein, B.B. Wolf, T. Kuwana, J.C. Goldstein, D.D. Newmeyer, R.C. Bleackley, D.R. Green, Granzyme B-mediated apoptosis proceeds predominantly through a Bcl-2-inhibitable mitochondrial pathway, J. Biol. Chem. 276 (2001) 12060–12067.
[49] K. Nagaoka, C. Sun, Y. Kobayashi, T. Kanaseki, S. Tokita, T. Komatsu, K. Maejima, J. Futami, S. Nomura, K. Udaka, H. Nakagawa, T. Torigoe, K. Kakimi, Identification of neoantigens in two murine gastric Cancer cell lines leading to the neoantigen-based immunotherapy, Cancers (Basel) 14 (2021) 106.
[50] J. Connors, D. Joyner, N.J. Mege, G.M. Cusimano, M.R. Bell, J. Marcy, B. Taramangalam, K.M. Kim, P.J.C. Lin, Y.K. Tam, D. Weissman, M.A. Kutzler, M.-G. Alameh, E.K. Haddad, Lipid nanoparticles (LNP) induce activation and maturation of antigen presenting cells in young and aged individuals, Commun. Biol. 6 (2023) 188.
[51] M.-G. Alameh, I. Tombácz, E. Bettini, K. Lederer, C. Sittplangkoon, J.R. Wilmore, B. T. Gaudette, O.Y. Soliman, M. Pine, P. Hicks, T.B. Manzoni, J.J. Knox, J.L. Johnson, D. Laczkó, H. Muramatsu, B. Davis, W. Meng, A.M. Rosenfeld, S. Strohmeier, P.J. C. Lin, B.L. Mui, Y.K. Tam, K. Karikó, A. Jacquet, F. Krammer, P. Bates, M. P. Cancro, D. Weissman, E.T. Luning Prak, D. Allman, M. Locci, N. Pardi, Lipid nanoparticles enhance the efficacy of mRNA and protein subunit vaccines by inducing robust T follicular helper cell and humoral responses, Immunity 54 (2021) 2877–2892.e7.
[52] E.A. Thoryk, G. Swaminathan, S. Meschino, K.S. Cox, M. Gindy, D.R. Casimiro, A. J. Bett, Co-Administration of lipid nanoparticles and sub-unit vaccine antigens is required for increase in antigen-specific immune responses in mice, Vaccines (Basel) 4 (2016), https://doi.org/10.3390/vaccines4040047.
[53] S. Ndeupen, Z. Qin, S. Jacobsen, H. Estanbouli, A. Bouteau, B.Z. Igyártó, The mRNA-LNP platform's lipid nanoparticle component used in preclinical vaccine studies is highly inflammatory, BioRxiv (2021), https://doi.org/10.1101/2021.03.04.430128.
[54] L.M. Howard, J.B. Goll, T.L. Jensen, K.L. Hoek, N. Prasad, C.E. Gelber, S.E. Levy, S. Joyce, A.J. Link, C. Buddy Creech, K.M. Edwards, AS03-adjuvanted H5N1 avian influenza vaccine modulates early innate immune signatures in human peripheral blood mononuclear cells, J. Infect. Dis. 219 (2019) 1786–1798.
[55] S. Khurana, E.M. Coyle, J. Manischewitz, L.R. King, J. Gao, R.N. Germain, P. L. Schwartzberg, J.S. Tsang, H. Golding, A. Biancotto, J. Candia, J. Chen, F. Cheung, H. Dickler, Y. Kotliarov, S. Perl, R. Shi, K.E.R. Stagliano, N.S. Young, H. Zhou, AS03-adjuvanted H5N1 vaccine promotes antibody diversity and affinity maturation, NAI titers, cross-clade H5N1 neutralization, but not H1N1 cross-subtype neutralization, npj Vaccines 3 (2018) 40.
[56] S. Morel, A. Didierlaurent, P. Bourguignon, S. Delhaye, B. Baras, V. Jacob, C. Planty, A. Elouahabi, P. Harvengt, H. Carlsen, A. Kielland, P. Chomez, N. Garçon, M. Van Mechelen, Adjuvant system AS03 containing α-tocopherol modulates innate immune response and leads to improved adaptive immunity, Vaccine 29 (2011) 2461–2473.
[57] H. Tanaka, N. Takata, Y. Sakurai, T. Yoshida, T. Inoue, S. Tamagawa, Y. Nakai, K. Tange, H. Yoshioka, M. Maeki, M. Tokeshi, H. Akita, Delivery of oligonucleotides using a self-degradable lipid-like material, Pharmaceutics 13 (2021) 544.
[58] J. Anindita, H. Tanaka, T. Yamakawa, Y. Sato, C. Matsumoto, K. Ishizaki, T. Oyama, S. Suzuki, K. Ueda, K. Higashi, K. Moribe, K. Sasaki, Y. Ogura, E. Yonemochi, Y. Sakurai, H. Hatakeyama, H. Akita, The effect of cholesterol content on the adjuvant activity of nucleic-acid-free lipid nanoparticles, Pharmaceutics 16 (2024) 181.
[59] T. Korzun, A.S. Moses, P. Diba, A.L. Sattler, O.R. Taratula, G. Sahay, O. Taratula, D. L. Marks, From bench to bedside: implications of lipid nanoparticle carrier reactogenicity for advancing nucleic acid therapeutics, Pharmaceuticals (Basel) 16 (2023) 1088.
[60] C.-H. Koh, S. Lee, M. Kwak, B.-S. Kim, Y. Chung, CD8 T-cell subsets: heterogeneity, functions, and therapeutic potential, Exp. Mol. Med. 55 (2023) 2287–2299.
[61] Y. Lin, Y. Song, Y. Zhang, X. Li, L. Kan, S. Han, New insights on anti-tumor immunity of CD8+ T cells: cancer stem cells, tumor immune microenvironment and immunotherapy, J. Transl. Med. 23 (2025) 341.
[62] M. Roerden, A.B. Castro, Y. Cui, N. Harake, B. Kim, J. Dye, L. Maiorino, F.M. White, D.J. Irvine, K. Litchfield, S. Spranger, Neoantigen architectures define immunogenicity and drive immune evasion of tumors with heterogenous neoantigen expression, J. Immunother. Cancer 12 (2024) e010249.
[63] K. Feng, X. Zhang, J. Li, M. Han, J. Wang, F. Chen, Z. Yi, L. Di, R. Wang, Neoantigens combined with in situ cancer vaccination induce personalized immunity and reshape the tumor microenvironment, Nat. Commun. 16 (2025), https://doi.org/10.1038/s41467-025-60448-3.